Drew University

College of Liberal Arts

Photooxidation of methoxyphenols on titanium dioxide aerosol surrogates

by

Nicholas Chiappini

Submitted in Partial Fulfillment

of the Requirements

for the Degree of

Bachelor in Arts

With Specialized Honors in Chemistry

May 2014

Photooxidation of methoxyphenols on titanium dioxide aerosol surrogates

*Nicholas Chiappini, Ryan Z. Hinrichs**

Department of Chemistry, Drew University

Abstract

Titanium dioxide, or rutile, while relatively uncommon in the atmosphere, has gained relevance in urban atmospheric chemistry over the past few decades due to its use in solar self-cleaning coatings for buildings and windows. Though it has not often been thought of as a component of classical aerosols, its remarkable photochemistry makes a strong case for reconsideration. Upon adsorption onto rutile aerosols or surfaces in the presence of oxygen, water, and sunlight, methoxyphenols were found to degrade via radical photo-oxidation to commodity chemicals and reactive aldehydes such as vanillin and coniferyl aldehydes. While these reactions appear often in the literature in suspension phase, heterogeneous gas-solid interface radical oxidation is markedly less common and nearly non-existent for the particular system studied. The radical oxidation processes observed form reactive species that may be active participants in browning reactions decreasing aerosol reflectivity. If this proves to be true, then photocatalytic aerosol components such as rutile must be included in atmospheric modeling to reduce the ambiguity of current models. Additionally, the reaction presented provides a far greener route to valuable commodity chemicals than currently used industry standards, reducing environmental impact of their production.

Table of Contents

Table of Figures and Schemes

1. Introduction

Thought to have been first coined during World War I by Frederick Donnan[1], the term aerosol refers to particles of a solid or liquid suspended in a gaseous medium. Aerosols fall under a broader class of mixtures known as colloids, microscopic dispersions of one state of matter within another. In the latter half of the 20th century, aerosols began to draw immense interest due to their, at the time, unclear implications and effects on anthropogenic, or human caused, climate change and atmospheric chemistry.[2] Stratospheric ozone depletion was a major realization that aerosols could affect atmospheric chemistry. The variety of sources from which aerosols can stem is vast, ranging from human sources such as industrial smoke and soot, to airborne mineral dusts. While these classes seem relatively simple, most aerosols found in the atmosphere are not homogenous, but rather conglomerates of many of the aforementioned types[3].

Depending on the source material, aerosols can induce differing climatic effects[2]. High albedo, or highly reflective, aerosols, derived in part from sea salts, mineral dusts[4] and sulfates, reflect a large fraction of incident solar radiation, thus exhibiting a net cooling effect on the atmosphere. Lower albedo aerosols such as black carbon derived from incomplete combustion of petroleum and other fossil fuels, and some brown carbons, organics derived from biomass combustion coated on other aerosols[5], absorb most or part of this incoming radiation and reradiate it as heat, thus producing a net warming effect on the atmosphere. This is in principle similar to the greenhouse effect of carbon dioxide and other gases often discussed as the agents of climate change, albeit with solid, liquid, and mixed particles rather than gases. Rather than absorbing outgoing IR radiation however, aerosols absorb incoming UV/Visible radiation. Despite these seemingly simple effects, lack of understanding of aerosol lifetime, chemistry, and effect of composition on both of these factors leaves a large amount of uncertainty in atmospheric models.

While balancing net warming and net cooling effects have far reaching impacts on the direction of anthropogenic and non-anthropogenic climate change, one aspect of these aerosols that remains comparatively unexplored is the heterogeneous chemistry that occurs at their surfaces. This chemistry could hold the secrets to particle growth in the atmosphere, the atmospheric gas budget, and how changes in particle albedo proceed. Particle growth refers to change in size of aerosols, such as the accretion of water around a dust particle in rain formation. The atmospheric gas budget refers to chemical regulation of the amounts of certain minority gases such as ozone (O_3), nitrogen dioxide (NO_2) and nitric oxide (NO) . As such, the topic has sparked a great deal of interest in the physical, atmospheric and organic chemistry communities. Because of the huge number of possibilities afforded through this model, chemists have attempted to model a number of heterogeneous reactions of this type such as nitration of aryl compounds[6] and ozonolysis of aryl compounds[7] adsorbed on sea salt aerosols, along with aging of organic adsorbents by gas and solution-phase reaction with ammonia[8] . The organics used in these studies were often those derived from the pyrolysis of lignin[9]. Lignin (Figure i) is a biopolymer found in the woody parts of plants which consists of methoxyphenolic and phenolic units.

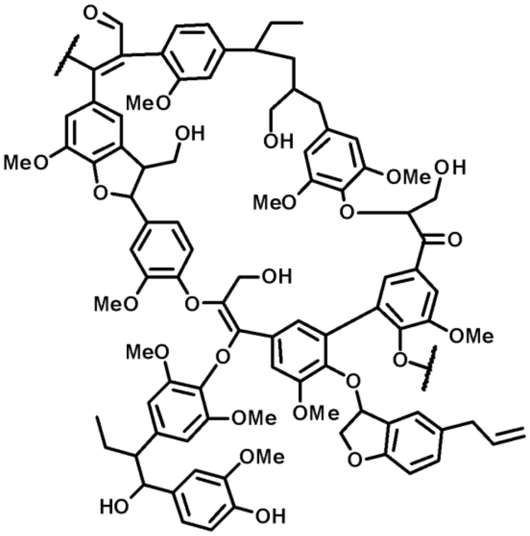

Figure i. A sample woody lignin polymer is shown. Note the large number of complex methoxyphenol and phenol substituents. Adapted from the polymer shown in Shen et al.[9]

Lignin contributes to wood's strength and rigidity. Due to the high degree of heterogeneity in the lignin polymer itself, upon pyrolysis a multitude of phenolic and methoxyphenolic compounds are produced, a sample set of which are shown in Figure ii.

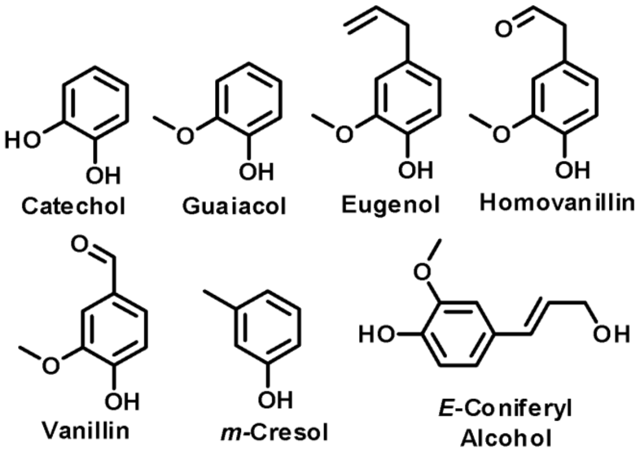

Figure ii. Various phenols and methoxyphenol derivatives

These and other so-called lignin pyrolysis products are abundant in arboreal environments and are produced *en masse* during forest fires. A number of these compounds are classified as semi-volatile organic compounds (SVOCs) due to their intermediate volatility (boiling point = ~150^{o} C - 300^{o}C) at ambient atmospheric conditions. Comparatively, very volatile and volatile organic compounds (VVOCs and VOCs) have boiling points between ~0-50°C and ~50-150°C respectively. These species are often found almost exclusively in the gas phase and do not condense as readily as SVOCs at atmospheric pressure (101.3 kPa). The semi-volatility of SVOCs allows them to easily adsorb from the gas phase onto aerosol surfaces. When combined with their variety of functionalities, this makes them prime targets for studies on reactivity in these systems.

As a logical extension of the results achieved by Woodill and Hinrichs[6] and Barnum, Medeiros and Hinrichs[7], other reactions of organics adsorbed onto mineral aerosols were investigated. O'Neill, Kawam and Hinrichs[10] demonstrated ozonolysis occurring upon surface adsorption of eugenol (2-methoxy-4-allylphenol) and 2-methoxy-4-propylphenol substrates on both sea salt (NaCl, KI) and mineral aerosol (Al_2O_3) surfaces[10] producing both ring-cleaved and side chain cleaved products as seen in Figure iii.

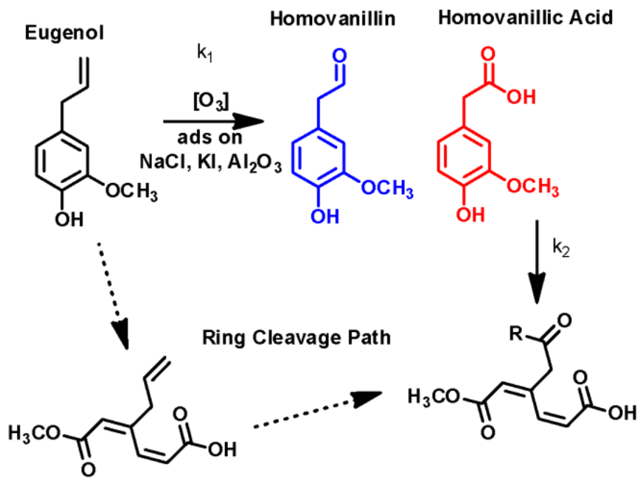

Credit: O'Neill, E., Kawam, A. 2012

Figure iii. Generalized reaction scheme of the ozonolysis of surface adsorbed eugenol on sea salt and mineral oxide substrates.[9]

Based upon these data suggesting similar products form on the mineral oxide and sea salt aerosol surrogate surfaces, investigations were launched into a unique type of mineral oxide, TiO_2 (rutile). Rutile is a well-established photocatalyst employed in many fields, being used heavily in urban environments for amenities such as self-cleaning windows[11], purification of water, and photochemical evolution of hydrogen (producing hydrogen by cleaving water with light) [12]. The photocatalytic activity of TiO_2 is due to its various semiconductor properties, including most critically, a small band gap[12,13]. As seen in Figure iv below, the compound's small band gap allows ultraviolet light to excite electrons originating in the valence band from surface bound molecules into the conduction band. The valence band and conduction band are concepts arising from molecular orbital theory applied to bulk solids. Basically, when viewing the molecular orbitals of these bulk solids, the orbitals separate into two groups: the bonding (electron-bearing) orbitals coalesce into the valence band, while the antibonding (electron-free) orbitals form the conduction band. In metals, the two bands are continuous. In non-metals, they are separated by a large gap, called a band gap which is insurmountable by the electrons even when excited by UV light or heat. In semiconductors, the band gap is small enough such that an electron can be promoted to the conduction band by a comparatively small amount of energy. In photocatalysts such as rutile, this energy comes from UV light. Rutile's bandgap has some range due to microvariations in crystal structure but lies between 3.12 eV (395 nm) 3.05 eV (407 nm) typically.[13]

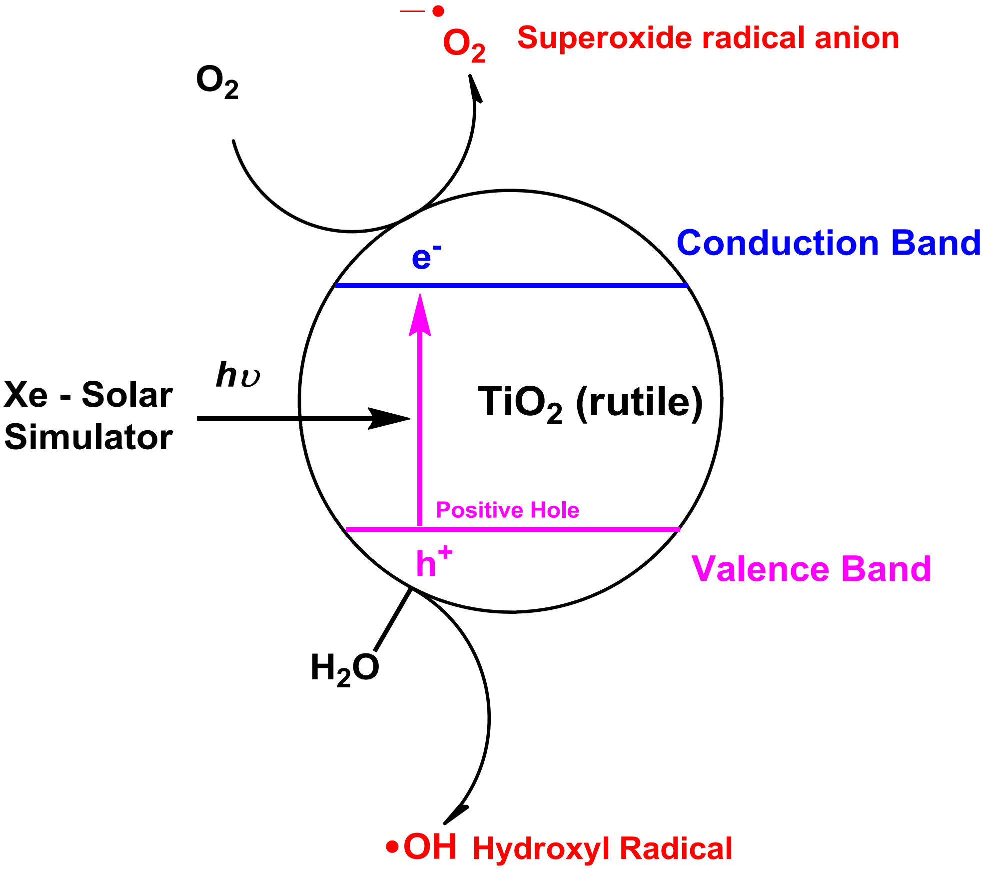

Figure iv. A diagram of the chief mechanism of photocatalysis in rutile titanium dioxide adapted from Nakata and Fujishima[12] , and Hirakawa et al.[14] Ultraviolet radiation promotes electrons in the valence band (including those from surface bound H_2O) to the conduction band. Once in the conduction band, the highly energetic electron attacks and reduces labile atmospheric molecules such as molecular oxygen to their corresponding radical anion. The promotion of the election from the valence band oxidizes the surface bound water to a hydroxyl radical which can then attack surface bound organic molecules.

This creates positive electron “holes” while liberating radicals of the surface bound molecule, most commonly water. The promoted electron residing in the conduction band is highly energetic and very easily reduces labile gaseous molecules such as molecular oxygen to the superoxide radical anion. Though many of the details concerning the mechanisms by which these radical species then proceed to attack surface bound organics is still unclear, some insight into the particular mechanism of organic decomposition and reaction on TiO_2 have been examined.

Since its discovery as a photocatalyst, TiO_2 has earned a reputation as the übermensch of photocatalysts due to its ability to degrade nearly any organic substrate given enough time[15]. Aliphatic hydrocarbons tend to begin reaction by losing an electron to the positive hole generated after activation of the photocatalyst, or to hydrogen abstraction by hydroxyl radicals (Scheme 1).

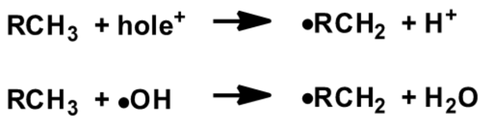

Scheme 1. An aliphatic hydrocarbon reacts with a positive hole or hydroxyl radical to general a reactive hydrocarbon radical.

They then continue forward with oxidation via adduct formation with molecular oxygen, termination with a hydroxyl radical, or reaction with other organic substrates[16,17]. The most common pathway for these oxidation reactions of aliphatics is the formation of an alcohol, followed by further oxidation of the alcohol if possible (Scheme 2).

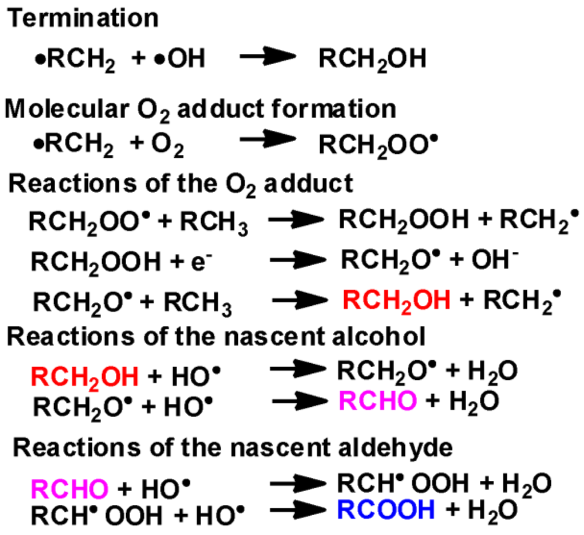

Scheme 2. After forming the alkyl radical, the compound can undergo addition of O_2 which can, in a few reactive steps, form the alcohol (red), the aldehyde (magenta), and the carboxylic acid (blue). Secondary alcohols form ketones when oxidized further[15,16].

Aromatic compounds exhibit similar oxidative reaction habits under these conditions. The general scheme of these types of reactions at aromatic sites entails activation of the ring by positive hole electron abstraction, followed by adduction with molecular oxygen or surface bound oxygen, and finally elimination of water to produce the aromatic alcohol[14] (Scheme 3).

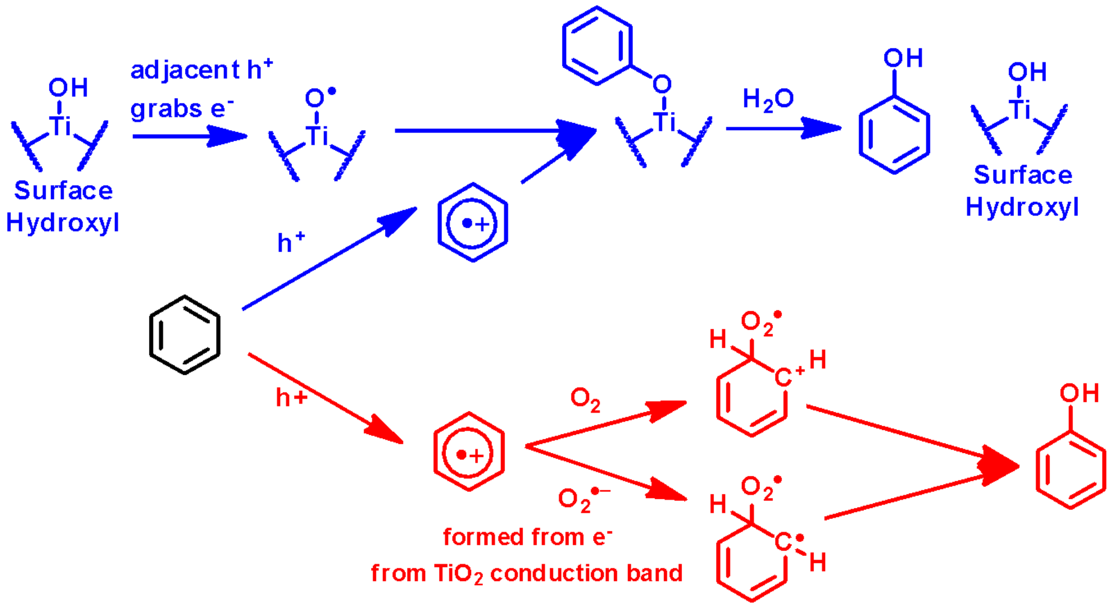

Scheme 3. The mechanism for water oxygen (blue) and molecular oxygen (red) incorporation in the oxidation of benzene as presented by Bui et al.[17] is presented. Notably, the water incorporation mechanism does not break the ring's aromaticity as the O_2 does.

It was realized that the oxygen used in the oxidation came from both water and molecular oxygen sources after isotopic studies performed by Bui et al.[18] showed that the end products of prolonged oxidation to CO_2 afforded mixed isotope CO_2 ($C^{16}O^{18}O$) when only $^{18}O_2$ or $^{18}OH_2$ was used, but monoisotopic CO_2 ($C^{18}O_2$ only) when both were used. This supports a similar mechanistic thread as was seen in oxidation of aliphatics by Blount et al.[15] and Ye et al.[16] insofar as oxygen from both O_2 and H_2O is incorporated into the observed products. Interestingly, the degree to which each contributed to the observed product oxygen was heavily dependent on the crystalline form of TiO_2 used with rutile showing 20-40% of product oxygen atoms from water following suspension-phase oxidation, and anatase showing 70-90% of product oxygen from O_2[17].

Expanding upon these first principles, chemists have utilized the oxidative power of suspensions of TiO_2 in water to produce a number of commercially relevant compounds from inexpensive starting materials in a far greener manner than otherwise possible[19], tuning reaction conditions to achieve maximum selectivity and yield of the desired compound. This type of oxidation has been used for reactions such as the mineralization of benzene[17] as shown previously, production of vanillin[18] and other flavorants[14].

Because of the immense amount of interest in and profit available from research into the photocatalytic properties of suspension-phase TiO_2 particles, there has been comparatively less research on reactions occurring at gas-surface interfaces. Gas-surface interface chemistry plays a critical role in the atmosphere as it is the primary mode of reactivity for aerosol adsorbed compounds. These types of chemical systems are particularly intriguing and poignant from an atmospheric perspective, as they represent one of the largest areas of uncertainty in climatic modeling, and chemodynamics of the lower atmosphere.

As mentioned previously, in the work of Woodill and Hinrichs[6], Barnum, Medeiros and Hinrichs[7], and O'Neill, Kawam and Hinrichs[10], the class of compounds known as lignin pyrolysis products react interestingly with atmospheric gases at these gas-surface interfaces on sea salts and clays, affording reactions such as nitration[6,7], oxidation[7], and ring-cleavage[10]. As a system of comparison for this previous work, reactions of lignin pyrolysis products on mineral oxides, namely the photocatalyst, TiO_2, were examined. Unlike the bulk of the literature on TiO_2's synthetic utility, this study chose to examine the oxidative power of photo-exposed TiO_2 on the lignin pyrolysis products, eugenol, 4-propylguaiacol (4PG), and 4-methylguaiacol. Reaction kinetics of surface oxidation of these methoxyphenolic compounds were studied at varying temperature, humidity, and oxygen concentrations using diffuse reflectance infrared Fourier transform spectroscopy (DRIFTS), attenuated total internal reflectance infrared spectroscopy (ATR), and gas cell infrared spectroscopy. The photoreactions of both eugenol and 4-propylguaiacol on rutile TiO_2 were found to have dependence on both oxygen and humidity for any appreciable change in surface IR absorption profile. Upon repeating initial trials of the photochemical oxidation of 4PG[20] with an atmosphere humidified with D_2O, the reaction rate was seen to decrease significantly[17]. This implies that the reactive species taking part in the oxidative process is dependent on the lability of the H-O or D-O bond. Of the two reactive species produced by irradiation of rutile suggested by Hirakawa et al.[13], this suggests that the hydroxyl radical, rather than the superoxide radical anion takes a leading role in this catalytic mechanism. DRIFTS[21] studies showed interestingly that over the course of the experiment, the 1505 cm^{-1} band assigned to the breathing C=C vibrational mode of eugenol's aromatic ring disappeared nearly completely by the 100 minute time point being replaced with a pair of strong bands at 1725 cm^{-1} and 1643 cm^{-1} which dissipate by the 800 minute time point. Because of this, it was inferred that these peaks were characteristic of reactive intermediates or oxidation products of eugenol and the hydroxyl radical. Unlike the condensed phase products seen in O'Neill, Kawam, and Hinrichs[10], these reactive intermediates react further and are consumed to presumably produce gaseous products that may correlate with compounds observed in HPLC studies by Peiró et al.,[22] aqueous suspension studies performed by Augliaro et al.[23], and mineralization by radical oxidation studies by Bui et al.[24] Gas-phase product studies show that the chief gaseous product of the reaction was carbon dioxide rather than formyl or acetyl compounds as initially theorized. To help elucidate the reactions occurring, condensed-phase product assays were performed on a much larger (10-20x) scale and analyzed using GC-MS in tandem with ^{1}H- and ^{13}C-NMR. Expanding the original scope beyond eugenol, the reactivities of other functionalized lignin pyrolysis products were analyzed using the same experimental technique. This photochemical route of oxidation without ozone will be compared and contrasted with ozonolysis, nitration, and other heterogeneous reactions.

2. Photo-oxidation of Methoxyphenols on Rutile

2.1 Methods of Product Characterization

2.1.1. Infrared Spectroscopy

Identification of condensed phase products and reaction kinetics for this study relies immensely on infrared (IR) spectroscopy. Infrared spectroscopy is built upon the basis that the energies of transitions between varying vibrational energy levels in a molecule fall within the range of infrared light (wavelength: 700 nm – 1 mm). When recording an infrared spectrum, infrared radiation is, depending on the specific type of IR spectroscopy, passed through a sample (transmission), impacts a sample on a crystal (ATR), or impacts a sample in a holding chamber, then collimated to an output beam. The difference between the radiative power input (I_0) and outputs (I) at various wavelengths appear in spectra as bands of absorption. This can be summarized in the generalized formula for absorbance shown below in Equation 1.

$$Absorbance = \log\frac{I_0}{I}$$

Equation 1.

Because IR looks specifically at the vibrational energy levels of a molecule, one can examine distinct stretching vibrations, which occur along a bond axis, and bending vibrations, which occur perpendicular to a bond axis to identify functional groups present in a sample by their unique energies. IR follows a quantum selection rule stating that absorptions only appear for vibrations which induce a net change in the electronic dipole moment of a molecule, meaning perfectly symmetric linear molecules such as N_2‘s stretching vibration are invisible. Frequency of vibrations for a certain bond can be described using the classical description of a bimolecular system as two masses on a spring. Frequency of vibration (v) is related to the effective spring constant (k), a measure of bond strength, and the reduced mass (μ) by the equations shown below in Equation 2.

Equation 2.

$$\nu = \frac{1}{2\pi}\sqrt{\frac{k}{\mu}}$$

$$\mu = \frac{m_2 m_1}{m_1 + m_2}$$

Stretching vibrations tend to induce far larger changes in dipole than bending vibrations and appear as more intense absorption bands. Because of this, stretching vibrations are more often used to easily characterize compounds.

In atmospheric chemistry, often the compounds of interest are complex organic (containing C-H) or inorganic (lacking C-H) mixtures, mimicking aerosol mixtures present in the Earth's atmosphere. Organic compounds lacking heteroatoms (atoms other than C or H) often lack distinct IR vibrations necessary for proper diagnostics, but because the primary chemistry studied in this thesis is oxidation of organic molecules, we circumvent this problem by looking to C-O, and C=O bonds, along with stretches in conjugated multiple bond systems as seen in eugenol in Figure 1.

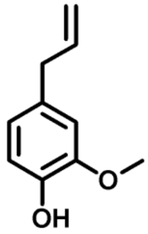

3618 cm^{-1} O-H Stretch
1514 cm^{-1} Aromatic Ring Breathing
1432 cm^{-1} C=C Symmetric Stretch
1268 cm^{-1} Aromatic Ether Stretch
1035 cm^{-1} Aromatic Ether Bend

Figure 1: Eugenol, a typical atmospheric organic molecule with some of its strongest IR active vibrations.

Unlike what is possible in metal carbonyl cluster chemistry, one cannot predict the number of stretching vibrations for complex minimally symmetric organic molecules using a group theory symmetry approach. Instead, when atmospheric chemists are interested in the theoretical IR spectrum of a compound, we must turn to the power of computational chemistry. Through the use of the program Gaussian, one can optimize the geometry of a compound using self-consistent field equations and density functional theory, then calculate all of the possible vibrational modes for that molecule. The downside to this approach is that with each atom added to the compound of interest, the calculation time increases greatly. A system of 22 atoms takes nearly a day of devoted calculation because the program ascribes a wavefunction to each electron in the molecule and attempts to find the most favorable solution to all of them, making the tasking almost Sisyphean for extremely complex molecules. Because of the tedium of this method, often times, it is much simpler to experimentally attain our answers, though Gaussian is incredibly helpful when identifying specific vibrational modes (Figure 2).

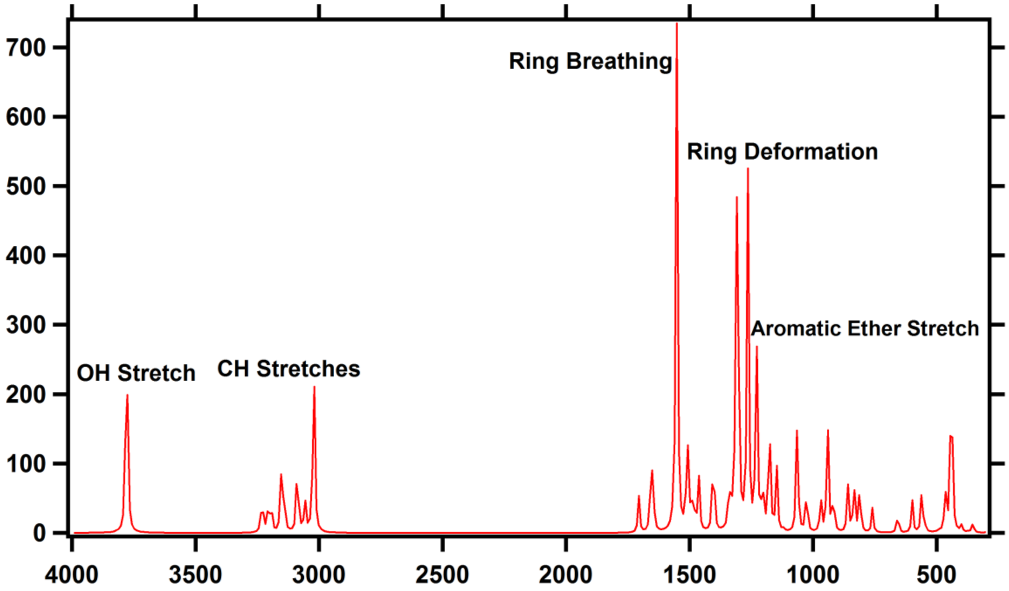

Figure 2. The gas-phase spectrum of eugenol as predicted by Gaussian (B3LYP/6-311G(d,p)++). Important regions of the IR spectrum are annotated with their associated functionalities.

Whenever there is a new compound of interest, the first experiment that is performed is a liquid film IR of the compound. One places a small amount of a liquid phase organic (or a solution thereof in a non-obstructing solvent, ex. CCl_4) between sodium chloride salt plates. A beam of infrared radiation is then passed through the sample, generating an IR spectrum as discussed previously (I_0 vs I). While the IR absorption bands attained from this method do not always reflect the IR absorptions seen when the compound is adsorbed onto a substrate of interest, this methodology gives us an approximation useful for tentative peak assignments later.

In this project we utilize a number of specialized forms of IR spectroscopy, namely DRIFTS (Diffuse Reflectance Infrared Fourier Transform Spectroscopy) and ATR (Attenuated Total Internal Reflectance). DRIFTS (Figure 3b) spectroscopy is markedly different than other types of IR spectroscopy. Rather than measuring a direct difference in power between the input and output IR beams, DRIFTS compares the power of IR beam scattering of an uncoated substrate to scattered radiation from a coated substrate, thereby providing a spectrum of the adsorbed organic. The Michelson interferometer (Figure 3a) allows a continuous IR source to be used. The resulting interferogram can then be deconvoluted by Fourier transform to produce an IR spectrum. This is true not only of DRIFTS, but all forms of FT-IR spectroscopy.

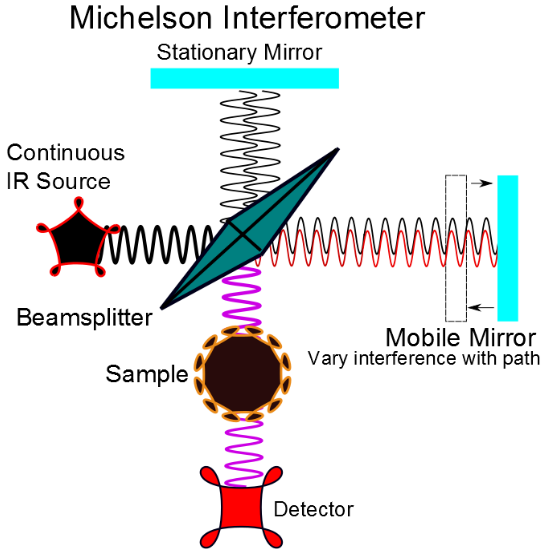

Figure 3a. A typical Michelson interferometer used for Fourier Transform IR (FTIR) is shown. A continuous IR source is split into two beams by a beamsplitter crystal (typically KBr) into two beams. These beams are directed towards mirrors, one stationary, one driven by a motor. The mobile mirror causes interference of the two beams upon recombination, producing an interference pattern. By averaging a large number of these interference patterns when analyzing signal from the detector, the computer can deconvolute the various signals or peaks of the IR spectrum from the interferogram.

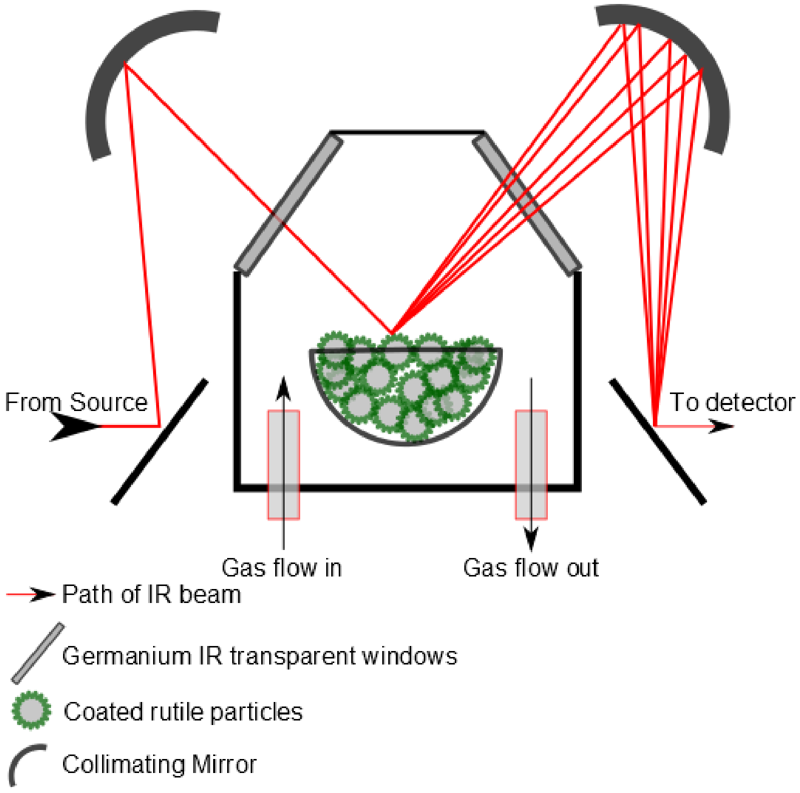

Figure 3b. A schematic showing the general logistics and functionality behind DRIFTS. An infrared beam is reflected onto a sample surface and some of the light is absorbed while most is reflected by faces and irregular surfaces of the solid. These diffuse beams are then recombined using a coalescing mirror into a coherent beam of infrared radiation which passes to the detector. Difference between the incident beam and the final beam show traces of what frequencies

ATR-IR functions differently still (Figure 4). An infrared beam is passed through a semi-conductor IR transparent crystal (zinc selenide or germanium) with a high refractive index, trapping the wave within the crystal. Despite the appearance of totally upending the traditional wisdom of measuring power difference to generate a spectrum, quantum mechanics dictates that a wave cannot be discontinuous at a boundary, allowing for a virtual wave, known as the evanescent wave, to enter the sample and be absorbed. ATR – IR works well with liquid or solid samples, but due to the short penetration distance of the evanescent wave (ca. 1 μm), sample thickness is limited.

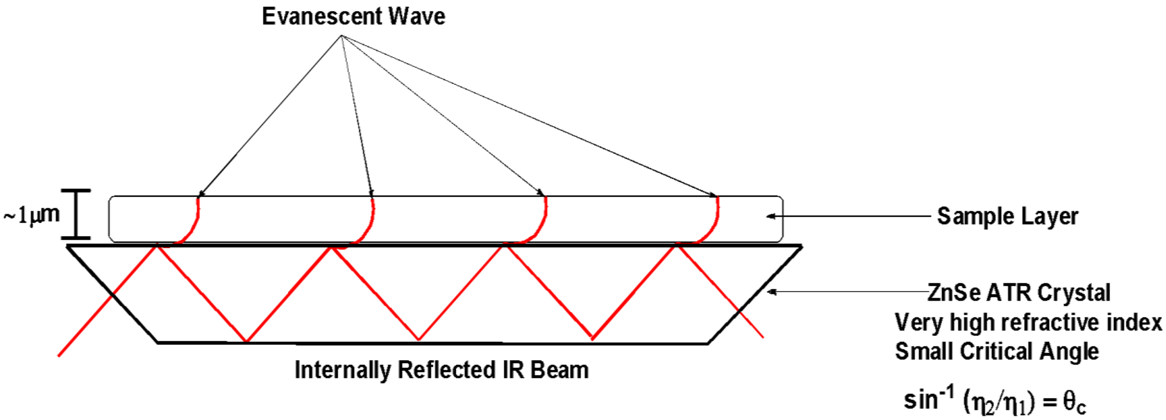

Figure 4. A schematic demonstrating the logistics of ATR-FTIR. An infrared beam is passed through a semi-conducting crystal which has a very high refractive index. Because of this, total internal reflectance in the solid is achieved with only a shallow critical angle. Quantum mechanics dictates that a wave function cannot be discontinuous at a boundary, creating a “virtual” or evanescent wave that penetrates into samples atop the crystal.

The third type of IR spectroscopy utilized in analysis of atmospheric systems is gas-phase IR spectroscopy. Gas cell IR works incredibly similar to the traditional transmission IR, but uses a sealed gas chamber with salt disc or IR transparent windows to allow the IR beam to pass through the sample. Because of its simplicity, gas cell IR will not be detailed further in this section.

2.1.2 Nuclear Magnetic Resonance Spectroscopy

Nuclear magnetic resonance spectroscopy (NMR) is a spectroscopic technique which utilizes the quantum mechanical property of spin, which is inherent to each and every nucleus. Normally, the spin states of a nucleus are degenerate, meaning that their energy is equivalent, however, when a strong external magnetic field (supplied by a superconducting electromagnet) is applied, these states split so that an energy gap exists between them; this is known as the Zeeman effect. Once the states are differentiated by this powerful magnetic field, a pulse of radio frequency excites nuclei from the lower energy spin state to the higher energy spin state. As these excited nuclei relax (return to) their original energy state, they emit radio frequency radiation which is registered by receiver coils around the sample (Figure 5).

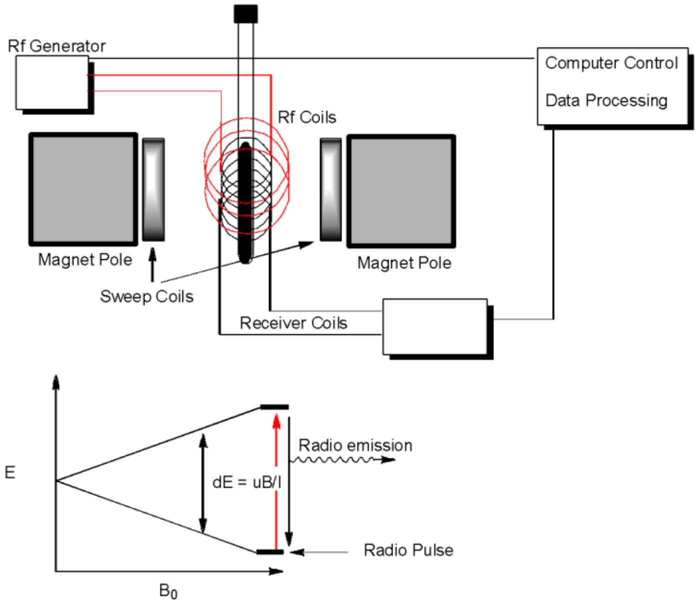

Figure 5. A schematic of a typical NMR spectrometer is shown above. An extremely powerful supermagnet surrounds the sample on all sides, generating a power field which causes splitting of nuclear spin states. The R_f coils generate the initial radio pulse that excites nuclei from the low energy to the high energy states. As the nuclei relax, receiver coils process the emitted radio waves into a readable NMR spectrum.

The energy of these emitted radio waves is determined by both the chemical and electronic environment around the nucleus of interest, causing, for example, hydrogens on different parts of a molecule to have distinct radio emissions. These emissions are separated from the jumbled output radio pulse or free-induction decay (FID) to give what is called an NMR spectrum, wherein frequency of an emitted radio pulse for a single nucleus is plotted against intensity. In addition to determining nuclear assignments based upon the frequency of the emitted radio pulse alone, one can also look at the splitting of peaks for information. Peak splitting occurs when a nucleus adjacent to the nucleus of interest interacts or *couples* with it, causing the peak to adopt an appearance based upon the number of other nuclei to which it is coupled (Figure 6).

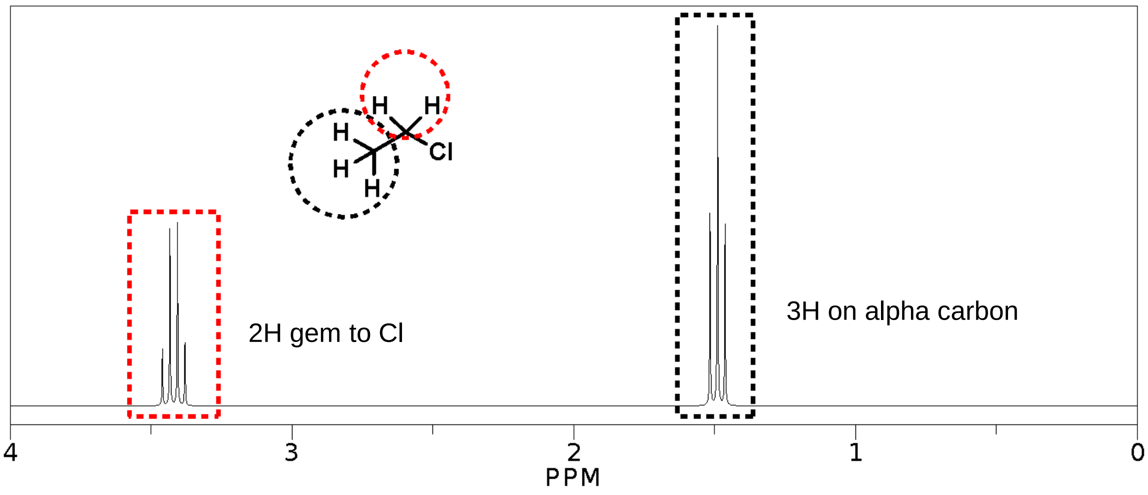

Figure 6. Shown as an example of NMR spectroscopy is the ^{1}HNMR spectrum of 1-chloroethane. Notice that the hydrogens circled in black correspond to the trio of peaks boxed in black. These hydrogens are split by 2 adjacent equivalent hydrogens on the second carbon, and thus show a triplet (2n+1). Conversely, the hydrogens denoted in red are split by 3 equivalent hydrogens, yielded a quartet (not the barbershop variety).

As an internal reference to keep spectra consistent between different instruments, the deuterium nucleus (^{2}H) is used to lock the magnetic field. Alongside this, the relative frequencies or chemical shifts of different nuclei within a molecule are referenced an accepted reference compound (TMS for ^{1}H, H_3PO_4 for ^{31}P, etc.).

Similar to the selection rules observed in IR spectroscopy previously, whether or not a nucleus is “NMR active” depends on its spin. If the nucleus has a non-integer spin value such a 1/2, 3/2, 5/2, which is true for the common nuclei ^{1}H, ^{13}C, ^{31}P, and ^{19}F, then the nucleus is considered NMR active. In this study, a combination of ^{1}H and ^{13}C NMR will be used to identify functional groups present in condensed phase products of photolysis, and to confirm product predictions based on gas chromatography mass spectrometry.

2.1.3 Gas Chromatography Mass Spectrometry

The third and final technique of analysis used in this project is gas chromatography (GC) mass spectrometry (MS). This technique is a combination of two different techniques. GC functions by flash-volatilizing a solution into the gas phase. Once in the gas phase, molecules move through a chromatographic column, a bound medium which separates compounds based on polarity and in GC, boiling point. A schematic of a typical GC-MS instrument is shown below in Figure 7.

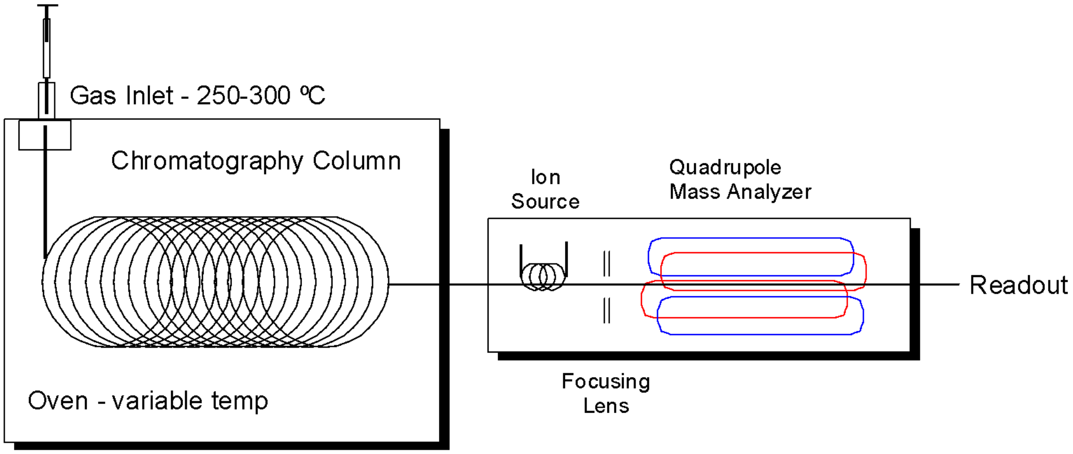

Figure 7. A typical Gas-Chromatograph with quadrupole mass analyzer detector. The quadrupole mass analyzer works by using alternating current on two of the poles (red), and direct current on the other two (blue). By varying the frequency of current applied.

Using this technique the components of a mixture can be separated into discrete peaks with unique retention times, or time spent on the column. Often, temperature is varied throughout a run to increase or decrease the speed with which a sample progresses through a column. By increasing the temperature, a linear increase in speed occurs; conversely, decreasing the temperature slows the progress of a compound through the column. Because it is common to have some compounds that elute, or leave the column, quickly and some that elute slowly, a gradient of temperature is used over the course of the run to better resolve fast eluting compounds and detect slow eluting compounds on a reasonable time scale. GC can use a number of different types of detectors to recognize when a compound is eluting, and in some cases, identify the compound from a chemical library. Some of the most common include a flame ionization detector (FID), which burns a sample utilizing a hydrogen flame and analyzes the resultant ions to generate a response or “peak” in the GC spectrum, thermal conductivity detectors (TCD) which pass eluting gas samples into a chamber of helium and measure the change in thermal conductivity to generate a signal, and finally mass spectrometry (MS).

Mass spectrometry ionizes eluted gases from the GC using either a powerful electron source (electron impact, EI), or chemical ionization (CI). These ionized species readily fragment into a plethora of molecular fragments due to the residual energy from ionization. This ionized mess of highly reproducible molecular fragments and molecular ions are then passed into a detector that selects based on mass to charge ratio. The most common type of detector used is what is known as a quadrupole. In a quadrupole detector four “poles” or metallic rods are connected to AC and DC current sources. The AC sources allow for rapid frequency switches in the generated magnetic field, causing particles to oscillate while travelling towards the detector. Only particles with just the right mass to charge ratio for the selected AC frequency will be allowed to pass into the detector. The instrument scans through a range of frequencies covering mass to charge ratios from 10 to 500 typically.

The real power of GC-MS comes from the output of the mass spectrometer for each peak observed in the GC chromatogram, or plot. By correlating observed fractioning patterns in the mass spectrum, one can infer the structure of the compound whose spectrum is being interpreted. The presence of certain atoms, such as bromine, is especially diagnostic due to having multiple isotopes with high natural abundance. If bromine is present in a compound analyzed by GC-MS, the MS spectrum will show two peaks of equivalent height for each fragment containing a bromine atom due to equal abundances of ^{79}Br and ^{81}Br. A large number of databases exist which can scan an inputted mass spectrum against a huge set of known compounds to provide closest known matches to the structure of the compound in that GC peak. Though powerful, GC-MS identification must be corroborated with secondary data such as NMR to confirm predictions by search algorithms. GC-MS is used in this project to quickly identify how many condensed-phase products are produced by the photolysis reaction.

2.2 Experimental

2.2.1 General experimental setup for IR Experimentation

Flow of carrier gas from a source tank of either air or nitrogen, is split by a T-junction into two flowmeters which regulate forward flow. The “dry” flowmeter circumvents a water bubbler and flows further into the system to a T-valve junction which can direct flow towards the reaction chamber or through a bubbler containing a semi-volatile organic liquid or solid. The “wet” flowmeter directs flow through a water bubbler which depending on the ratio of the flow rate of dry to wet, regulates relative humidity in the system. Both input streams join at a four-way junction which leads to the reaction chamber. The reaction chamber is designed with a bypass and valves allowing one to close or open flow in or out of the chamber. Outflow from the chamber flows into a vacuum trap, or in some cases, a gas phase IR cell (Figure 8).

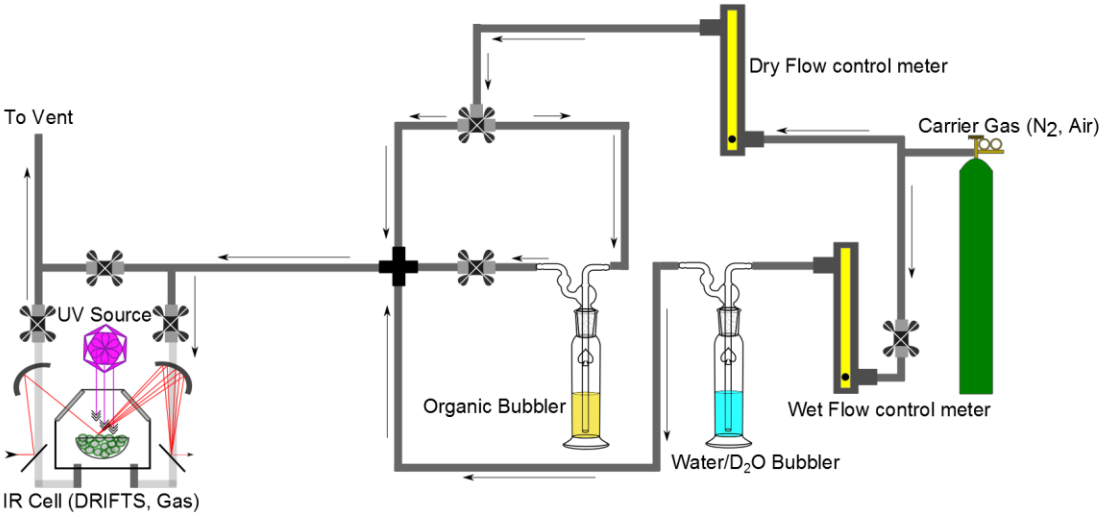

Figure 8. Standard experimental setup. All tubing except for that attached directly to the sample chamber and its valves, which was steel, was 3 mm gauge teflon. The various sample chambers were switched out at the two joints flanking the UV-Vis source indicated above.

2.2.2 DRIFTS studies of Surface Photochemistry

Samples consisted of 140.0 mg of rutile titanium dioxide (ball-milled 5 minutes) packed into the DRIFTS reaction chamber which were baked at 300ºC for 1 hour to remove adsorbed traces of water and other atmospheric contaminants. After cooling, samples were exposed to 50 to 74 standard cm^3 min^{-1} (sccm) of carrier gas directed through the organic bubbler under a dry atmosphere to ensure maximum adsorption of the organic compound for periods ranging from 60 to 160 minutes. Once coating was complete, the sample chamber was isolated as the system was opened to the water bubbler, then reopened during humidification to allow proper equilibration. Following equilibration to the desired relative humidity (RH%, usually 20-40%), the sample was exposed to UV irradiation from a Solar Works Solar Xenon Simulator (Emission profile shown in Figure 9a, comparative solar irradiance shown in

Figure 9b) with a water filter to remove IR for a reaction period of 800 minutes whilst infrared spectra were collected every 2.1-3.4 minutes (256 scans averaged per spectrum) of the sample at 4 cm^{-1} resolution on a Nicolet 6000 MCT-IR.

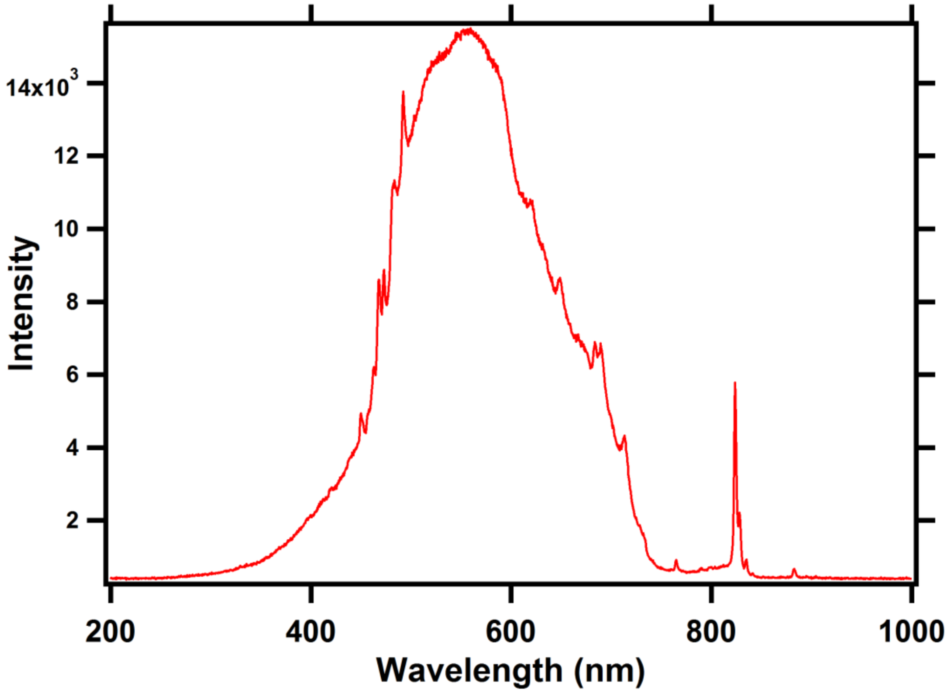

Figure 9a. The radiative output of the Xe solar simulator at wavelengths ranging from 200-1000 nm. Peak irradiance intensity occurs at 560 nm. This spectrum was recorded by feeding irradiance from the Xe solar simulator into the fiber optic detector of an OceanOptics USB4000-UV-Vis Miniature Fiber Optic Spectrometer which output data into a cohesive spectrum. Rutile has an ideal photoactive range below 406 nm.

Copyrighted Material Redacted

Please View Citation Provided to View Material

Figure 9b. Solar irradiance spectrum at sea level with the extraterrestrial (outside atmosphere) spectrum shown as a dotted line. Notably, the irradiance at sea level has a cutoff around 300 nm with maximum irradiance between 450-500 nm. The Xe-Hg lamp simulator mimics this spectrum well, having excellent overlap with the highest intensity regions of the spectrum. (Reproduced from Newport Solar Simulator Training manual, data reproduced from Sayre, R. and Kligman L., *Photochem. Photobiol.* **1992**, *55* (1) 141.)

Studies of radiant heating from solar irradiation suggest the simulator can raise the temperature of the sample to 50ºC, but this issue is addressed by cooling the DRIFTS sample cup with a constant flow of isothermal (25ºC) water throughout experiment. Incident radiant intensity was measured using a photometer to be 150 mW at the maximum intensity used. Control experiments were performed to test each variable. The importance of atmospheric oxygen was qualified through replicate experiments in which nitrogen was used as a carrier gas rather than air. Similarly, humidity's importance was qualified through use of dry (<5% RH) air during replicate experiments instead of the standard 20-40%RH. Kinetics of the reaction were probed through humidification of the system atmosphere with D_2O rather than water. From kinetic plots of characteristic peak loss, the kinetic isotope effect was able to be quantified for 4-propylguaiacol, a non-exocyclic alkene derivative of eugenol.

2.2.3 ATR IR studies of Surface Photochemistry

Samples consisted of approximately 5.5 mg of rutile titanium dioxide (ball-milled 5 minutes) coated onto the zinc selenide crystal surface as a highly viscous water slurry (approximately 3 sample masses of water were added to prepare the slurry). Once coated, the crystal was baked to dryness to produce a thin coating of rutile of nearly uniform thickness. Unlike in DRIFTS experimentation, samples were not baked as the coating process functionally removed surface adsorbed water through heating to dryness. Under a dry (<5% RH) atmosphere, samples were coated by a 74 sccm (standard cubic cm per minute) flow of dry air or nitrogen passed through the organic bubbler for 60 minutes. Similar to the DRIFTS technique, the chamber was isolated after coating, the system was opened to flow from the water bubbler, and the chamber was reopened once humidification began. After attaining the desired equilibrium humidity, samples were exposed to UV irradiation by a solar simulator for a period of 800 minutes while IR spectra were collected continuously every 1.4-3.1 minutes (256 scans averaged per spectrum, 4 cm^{-1} resolution, variance in time per averaged spectrum due to mirror velocity changes).

2.2.4 Gas-cell IR studies of eugenol and 4-propylguaiacol photoreactions

Samples consisted of on average 1.00 g of solid rutile powder placed in the bottom of the cubic gas cell as seen in Figure 5. The powder was then coated with eugenol over a two hour period, after which time the cell was sealed and the system was allowed to equilibrate. Reaction spectra were then recorded using the same Nicolet 6000 MCT-IR used in the DRIFTS reaction studies while UV radiation from a solar simulator bombarded samples in the sealed gas cell to monitor gas-phase product formation as shown in Figure 10.

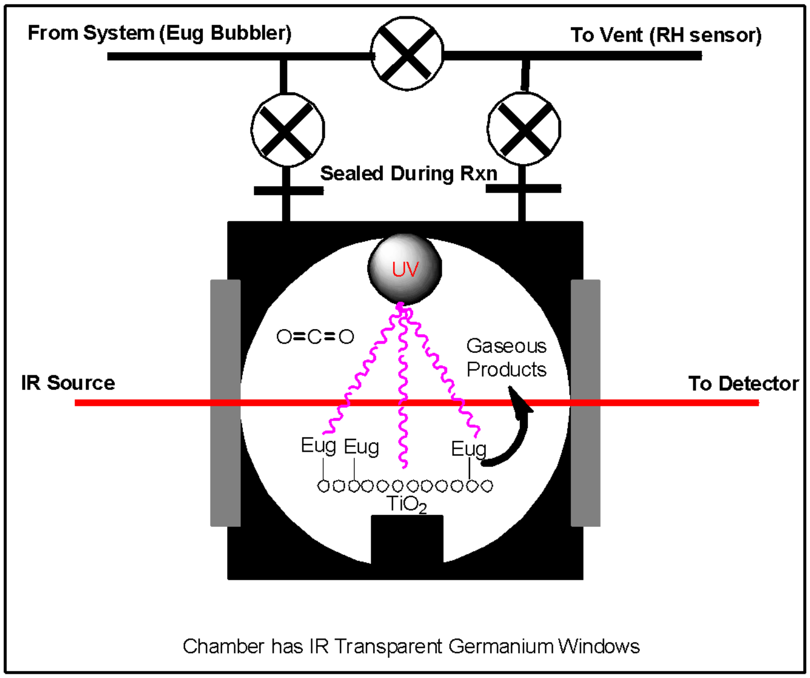

Figure 10. The gas-cell IR reaction chamber is shown. The base of the cell was coated with TiO_2

2.2.5 Condensed phase large-scale photoreaction of eugenol, 2-methoxy-4-propylphenol, and 2-methoxy-4-methylphenol

Unlike in the DRIFTS, gas-cell, and ATR studies, organics were coated onto the mineral oxide substrate using a liquid-liquid coating technique. To a 500 mL, three-neck round bottom flask were added dichloromethane (100 mL), rutile TiO_2 (1.00 g, 12.5 mmol, Aldritch) or α-alumina (1.28 g, 12.5 mmol), and the methoxyphenol of choice (0.174 mmol eugenol, 2-methoxy-4-propylphenol or 2-methoxy-4-methylphenol). The resulting heterogeneous mixture was sonicated in an ultrasonic bath (frequency = 30 kHz) for 1h to homogenize and emulsify the rutile particles while impregnating them with the organic of choice. The dichloromethane solvent was removed from this emulsion *in vacuo* (ca. 340 bar @ 40ºC) with a high speed of rotation to create a uniform coating of mineral oxide-organic particles on the walls of the glass bulb. Following this, saturated (ca. 100% RH) air was flowed through the bulb (ca. 0.5 ft^3 min) while the coated walls were irradiated from two sides by intense simulated sunlight (Figure 11).

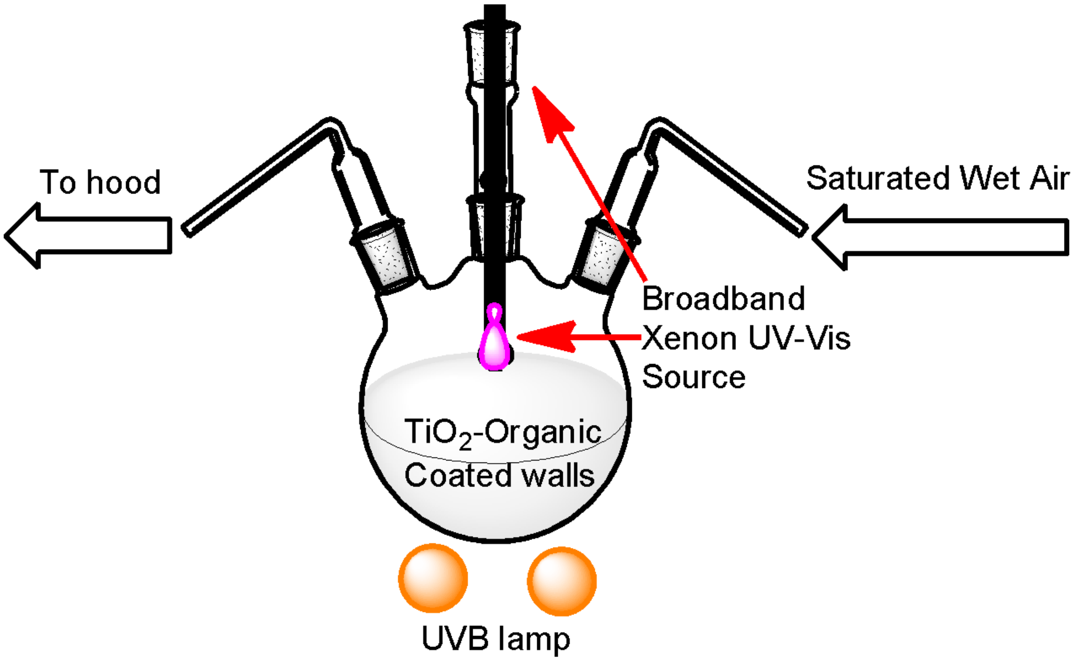

Figure 11. The standard experimental setup for condensed phase collection and identification experiments is shown. Water saturated air is flowed through the chamber with walls coated by TiO$_2$@organic particles while the sample is irradiated by two UV sources to ensure maximum surface area exposure to the UV.

Following irradiation for periods of 72 or 128 h (wanted to maximize the amount of product formed thus examined two extremes), the products were extracted into acetonitrile (100 mL), by sonicating the flask for 1 h. Spent titanium dioxide or alumina was then removed from the reaction mixture by filtration through a celite (diatomaceous earth) plug, affording a translucent solution ranging through various shades of yellow and beige. For GC-MS analysis of samples, this filtrate was concentrated *in vacuo* to approximately 5% of its original volume. For each sample to be analyzed, 1.0 mL of the concentrated filtrate was combined with 5 drops (1 drop ~ 0.05mL) of N,O-Bistrifluoroacetamide (BSTFA), a compound which converts free –OH, -NRH, and other labile hydrogens to stable trimethylsilyl derivatives. This derivitization serves a triple purpose: it lengthens the shelf-life of samples by removing a primary route of reactivity, it increases volatility of normally low-vapor pressure compounds, and it reduces tailing, or poor peak resolution in GC-MS . Because only a limited number of products were observed for the initial extraction of the 4-propylguaiacol photolysis products, a secondary extraction with acetonitrile spiked with 5 drops of BSTFA was performed, exposing hidden products that were too tightly bound to the surface for the mild extraction methods . For NMR analysis of samples, due to time constraints, concentrates from the GC-MS sample preparation were concentrated further to 20% of their previous volume to give a super concentrated sample. Approximately 0.1 mL of this highly concentrated sample was then combined with 0.6 mL of d_3-acetonitrile. Hydrogen NMRs(128 scans, TD = 1s, 300 K) were collected for the 4-propylguaiacol and 4-methylguaiacol extracts to corroborate structures predicted by the GC-MS search algorithm.

3. Results of Experimentation

3.1 DRIFTS[25] Continuous Flow Experimentation

3.1.1 Photooxidation on rutile proceeds through preliminary carbonyl intermediates

Using IR spectra of the eugenol-rutile surface recorded over 800 min of irradiation, reaction profiles and spectral features of possible products and/or intermediates were identified. Of particular note was the growth and subsequent decay of a peak cluster in the carbonyl region centered on 1725 cm^{-1}. This cluster was found to grow in rapidly within the first 100 minutes of irradiation, and then decay slowly for the remainder of the exposure period (Figures 12,13). Loss of the 1505 cm^{-1} peak was correlated with the total loss of eugenol over the 800 minute exposure window.

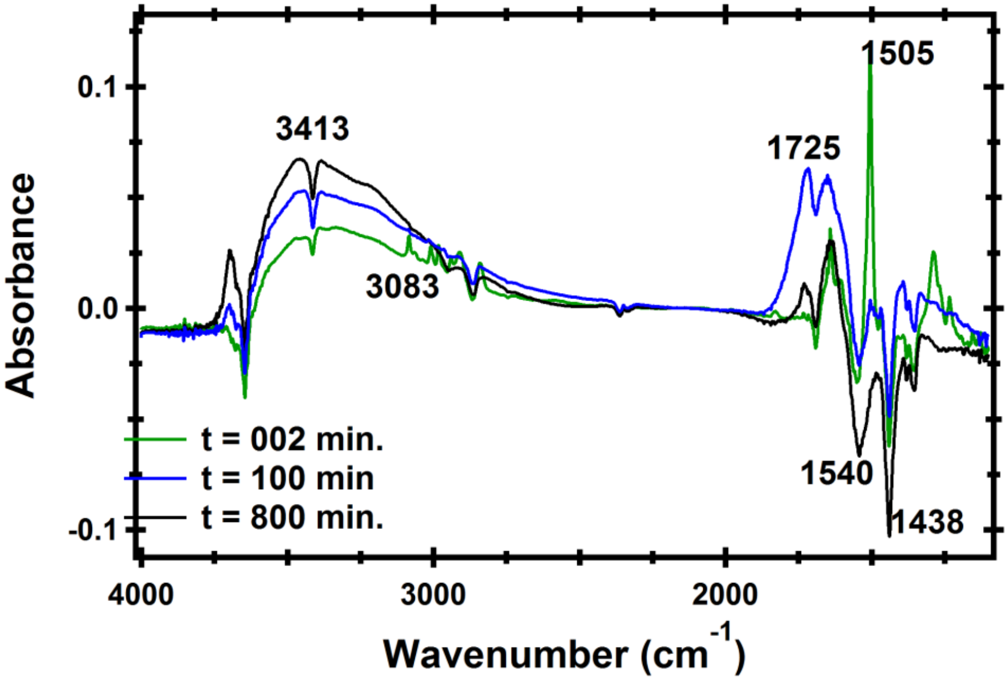

Figure 12. IR raw spectra of eugenol adsorbed on rutile exposed to UV irradiance for a period of 800 min are shown. Interestingly, a carbonyl region peak can be seen to grow in to a maximum at 100 minu and decrease over the remainder of the experiment. Key spectral features include the carbonyl band at 1725 and 1690 cm^{-1}, and the 1505 cm^{-1} band associated with the aromatic ring breathing stretching vibration.

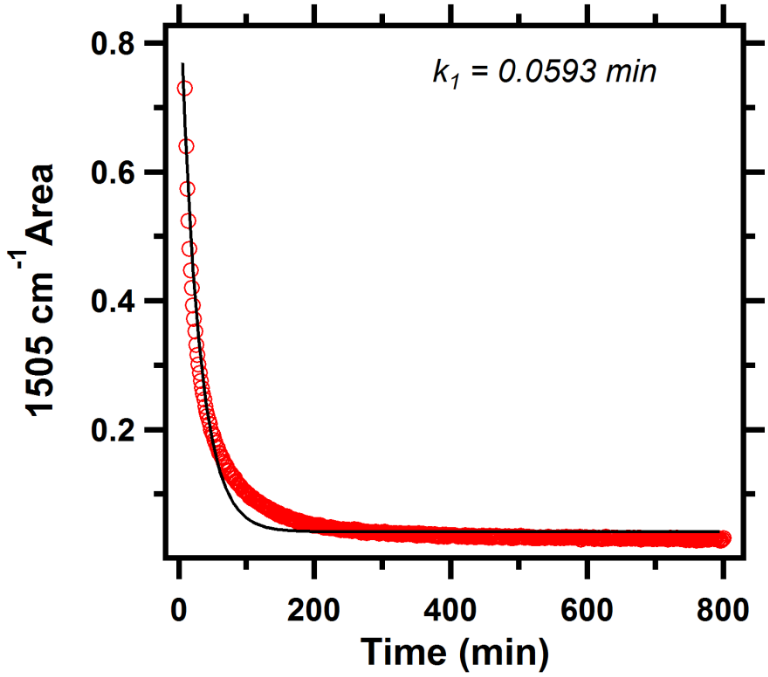

Figure 13. The kinetic loss profile of the 1505 cm^{-1} peak as a function of time is shown above. This is attained by integrating the 1505 cm^{-1} peak over the 800 minutes of experimentation. This is then fit with equation 3.

The kinetics analysis of the 1505 cm^{-1} peak was analyzed as a measure of how quickly eugenol was being consumed by the reaction occurring at the surface. This peak was chosen as it is characteristic of the aromatic stretching vibrations present in surface bound *para*-alkylguaiacol species, thereby loss of this peak indicates lack of conservation of this alkyl species. By tracking the kinetics of the loss of this spectral feature, one attains the rate of net loss of starting material without obstruction by intermediate formation. The kinetics of the 1505 cm^{-1} peak loss were characterized by fitting with the non-linear curve-fitting algorithm shown below in Equation 3 (y_0 = y-intercept, A_1 = preexponential factor, x_0 = x-offset, τ_1 = inverse of the rate constant).

Equation 3.

$$y = y_0 + A_1 \exp\left(\frac{x - x_0}{\tau_1}\right)$$

Following the characterization of this total metric for starting material loss, the formation of possible intermediates was probed by looking at the kinetics of the 1725 cm-1 peak which grows in and then decays (Figure 14). Integration of this peak over the time frame of experimentation shows a curve indicative of a sequential mechanism, i.e. a fast initial reaction forms an intermediate and a slower secondary reaction consumes this intermediate. To characterize the relative rates of these processes, the kinetic profile was fit using double exponential with constant x-offset algorithm in IGOR-Pro shown below in Equation 4.

Equation 4.

$$[I] = \frac{k_A}{k_I - k_A}\left(e^{-k_A t} - e^{-k_I t}\right)[A]_0$$

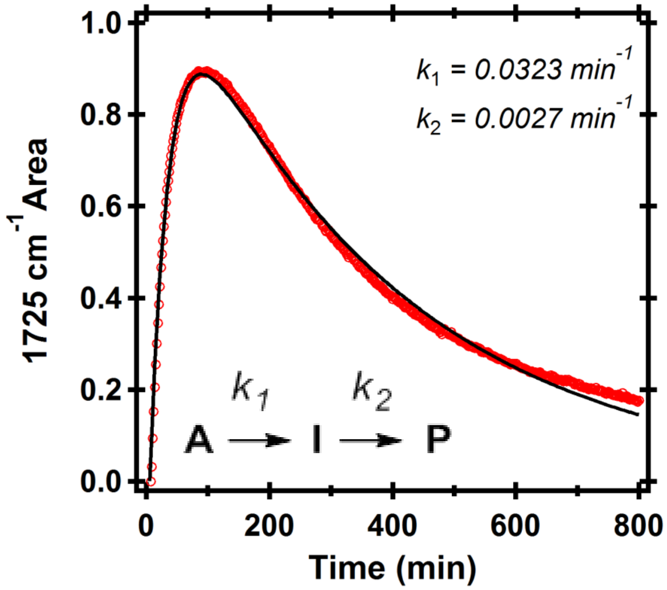

Figure 14. Sequential kinetics profile of the 1725 cm $^{-1}$ peak in the reaction spectra shown in Fig 12. The profile shows rapid growth of this carbonyl region peak within the first 100 minutes of exposure, with a secondary slower decay over the remainder of the 800 minute time window. This profile was surmised to represent formation of a product or intermediate followed by consumption by further oxidation.

As seen above, the 1725 cm^{-1} peak grows precipitously to its maximum at 100 min, followed by a gradual, slower decline over the remainder of the experimental window. Because two independent processes were expected to have caused this, sequential fitting done for the integration over the entire experiment resulting in two first order rate constants of 0.0323 min^{-1} for the formation region and 0.0027 min^{-1} for the region of consumption/desorption. Without the power of the non-linear curve-fitting afforded by Equation 4, resolving these two processes would require the use of a linearization technique such as the Lineweaver-Burke double reciprocal plot commonly utilized in biochemical kinetics.

To test this apparent photoreaction, one must examine the reaction for dependence on UV irradiation below the bandgap cutoff, oxygen, and water in addition to kinetic probing of rate determining step via isotopic studies.

3.1.2 UV radiation below 350 nm is necessary for rutile-methoxyphenol photochemistry

The first experiment performed as a control for the use of rutile titanium dioxide was an observation of the surface reaction of 4-propylguaiacol on the rutile substrate with and without irradiance in the UV region. Using a borosilicate glass slide as a low-pass filter, wavelengths below the measured cutoff of 350 nm were blocked, allowing only longer wave UV and visible light into the sample chamber. A thermocouple placed in the sample cup measured temperature in the sample to be approximately 50ºC after 100 minutes of irradiance both with and without the filter in place. Infrared difference spectra collected every 2.14 minutes recorded changes in the IR absorption profile of the adsorbed 4-

propylguaiacol over 110 minutes of irradiance in an air atmosphere (60 sccm). Difference spectra are produced by subtracting time point zero spectra from each new time point's spectrum. Studies of UV dependence were conducted under high humidity (ca. 45%), aerobic (air atmosphere) conditions. Of great interest in these experiments was the time evolution of the carbonyl and aromatic region of the IR spectrum as suspected products of photocatalyzed oxidation chiefly involved loss of aromaticity and the formation of ketone, aldehyde, or carboxylic acid moieties. In the absence of the lower wavelengths of light cut off by the borosilicate glass, the rate of product formation was noticeably lower and a larger amount of methoxyphenol starting material was observed (1506 cm^{-1} ring breathing vibration of starting material). Looking to the IR spectra of the reaction at the 100 min time point spectrum as shown in Figure 15, one can see in the spectrum with the filter (blue) that the product signal (1720 cm^{-1} and 1620 cm^{-1}) is not nearly as strong as in the unfiltered spectrum (red). Additionally, comparing the aromatic ring breathing stretching vibration (ca 1506 cm^{-1}) characteristic of the starting material between the two, it becomes apparent that the filtered reaction occurred to a lesser degree than the unfiltered reaction.

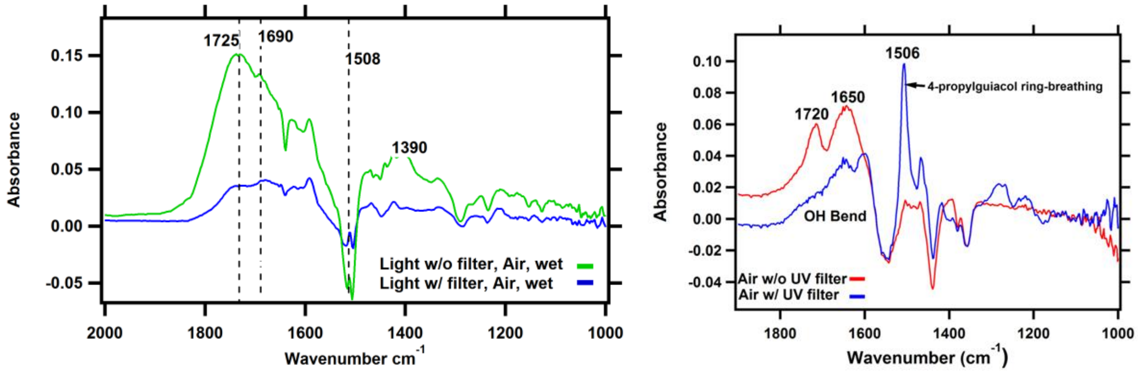

Figure 15. The 100 min time point IR spectra of 4-propylguaiacol on rutile under UV irradiance

with (blue) and without (red) a 350 nm borosilitcate filter are shown. The experiment with the filter showed a markedly lessened reactivity, with far less loss of the 1506 cm^{-1} ring breathing vibration, and less growth and definition of the peaks in the carbonyl region (1720 cm^{-1} and 1650^{-1}). Without the filter in place, the aromatic ring breathing vibration decreased substantially and peaks at 1720 and 1650 cm^{-1} were observed superimposed on the OH bend. Shown in green and blue on the left graph are the difference spectra of these same time points. Difference spectra are obtained by subtracting initial spectra from each successive time point spectrum.

What this told us about the reaction was that although the lower wavelength UV's absence did not completely stop the reaction from occurring; it did change the degree to which it occurred. Because the band gap of rutile occurs around 406 nm, meaning all shorter wavelengths of light shall be absorbed, it is intriguing that the experiment without wavelengths below 350 nm shows as large of an effect as observed.

3.1.3 Oxygen is critical for the photooxidation reaction on rutile

Following the observations suggesting that UV below the borosilicate cutoff (350nm) was necessary for photoreaction of guaiacol derivatives on the rutile surface, trials were conducted to test the oxygen dependence of the process. A lack of oxygen dependence would suggest a mechanism of oxidation solely dependent on water and its derivative species, while a positive result would suggest a more complex mechanism pending results of water dependence studies. To probe this question, samples of rutile were coated with eugenol via gas-phase adsorption and irradiated without a filter under air and nitrogen atmospheres with nearly identical humidities (27 ± 3%) for a period of 800 minutes (Figure 13). The reaction in air was observed to produce a pattern of peaks similar to that observed with the photoreaction of 4-propylguaiacol in the UV experimentation including a 1722 cm^{-1} peak in the mid-range carbonyl region, a low range carbonyl at 1693 cm^{-1} and a suspected aromatic band at 1623 cm^{-1}. Notably the original aromatic band of the guaiacol core with only alkyl substituents at 1508 cm^{-1} was observed to have been lost over the course of the 100 minute window. This loss was observed to be far more severe in the air atmosphere than in the nitrogen atmosphere, which showed little to no reaction as shown by the subtraction result spectra in Figure 16 below.

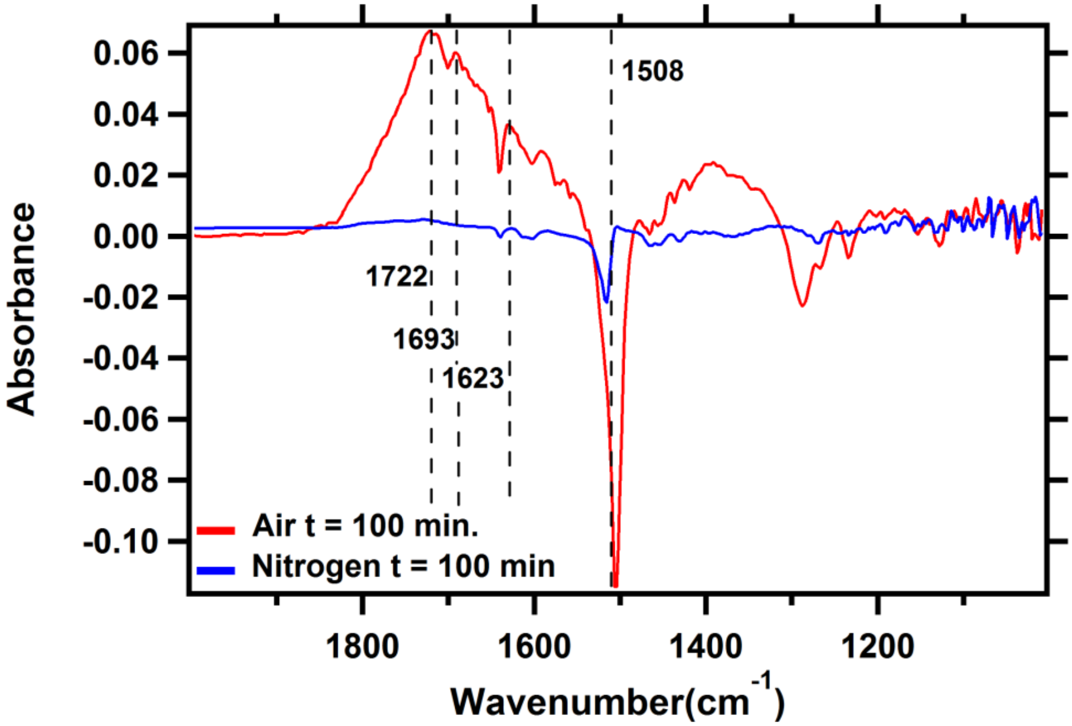

Figure 16. IR subtraction spectra of eugenol reacting on rutile with UV irradiance under nitrogen (blue) and air (red) atmospheres (27 ± 3% RH) are shown. The subtraction spectra were generated by subtracting initial spectra (2.14 min) from the 100 min spectra. Notable peaks include carbonyl region (1722 cm^{-1}, 1693 cm^{-1}), aromatic region (growth of 1623 cm^{-1}, loss of 1508 cm^{-1}). This spectral profile looks markedly different from the strict UV dependence due in part to humidity difference. One result observed consistently throughout experimentation was the humidity dependence on shape of the carbonyl region: at low (ca 5%) and high (ca 45%) humidities the carbonyl peaks were well defined, but at intermediate humidities (ca 20-30%), definition suffers. This may be due in part to transition between catalytic and bulk water properties on the surface.

From these observations, it seemed reasonable to conclude that the photo-oxidative process occurring at the rutile surface was dependent in large part on the action of molecular oxygen. Using this, we can infer that the mechanism of the oxidation reaction includes adduction or action of O_2 at some critical juncture.

3.1.4 Hydroxyl Radical Formation is a Rate Limiting Step in this Photooxidation Reaction

As a logical extension of the observation of O_2's critical role in the photo-oxidative process, the role of water in the mechanism was probed using variable humidity experimentation along with deuterium isotope labeled water experiments. Experimentation involving simple variance of humidity showed inconclusive results suggesting reaction efficacy was higher in higher humidity scenarios as seen in Figure 14. Interestingly, it seems that even in low humidity, where little loss of the ring breathing vibration at 1505 cm^{-1}, carbonyl formation is still observed at 100 min. This may suggest that the more likely oxidation pathway without excess water present is attack at the exocyclic alkene. By first reacting at the alkene, the coniferyl aldehydes shown as an inset in Figure 17, can form as persistent intermediates along the oxidation pathway to vanillin. This suggests, as expected, that water plays a key role in the reaction mechanism likely occurring in this system.

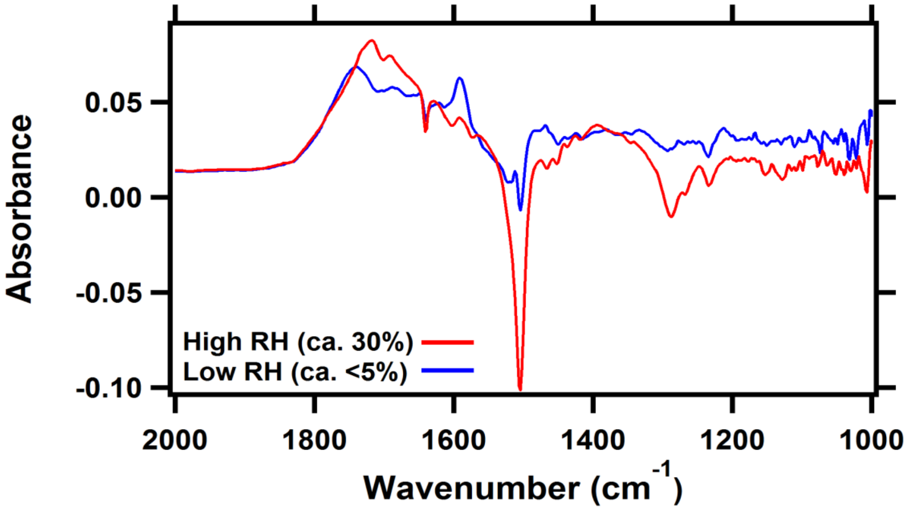

Figure 17. IR Cross sections of the carbonyl region for the photoreaction of eugenol on rutile at the 100 minute time point (red-high RH, blue-low RH). Notably the difference between the two is not readily apparent, possibly suggesting that only a catalytic amount of

water is necessary.

Despite the relatively inconclusive results seen with the relative humidity variation experiments, experimentation in which deuterated water (D_2O) was used in comparison to water (H_2O) showed a more decisive result. Growth of the carbonyl region in the deuterium experiments was significantly less rapid than that seen in the regular water trial as seen in Figure 18. Both trials reached carbonyl peak maxima at or near the 100 min time point as anticipated, though the magnitude of the carbonyl peak at the 100 min point relative to the 12 min time point was far less for the deuterium experiments.

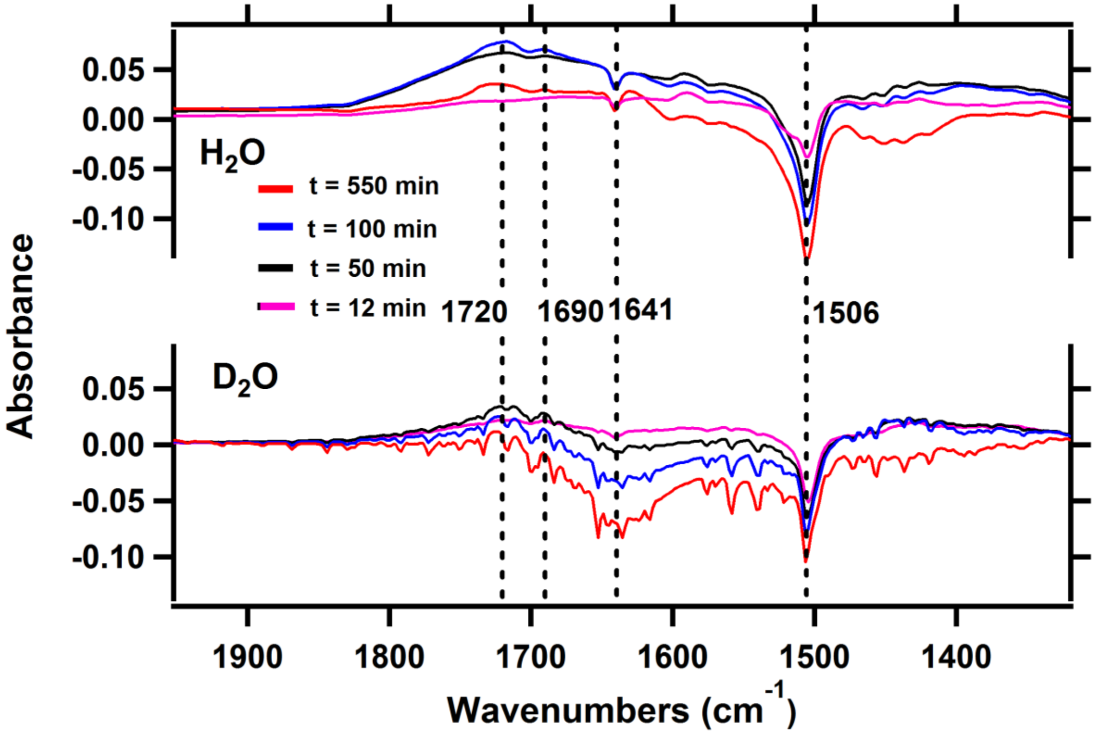

Figure 18. IR cross-sections of photoreaction of eugenol on rutile using water and deuterated water humidified atmospheres (25% RH for each). The growth of the carbonyl region continues until a maximum at or near the 100 min time point, followed by a decrease following this.

Clearer results were attained when the experiment was replicated with the compound 4-propylguaiacol, a methoxyphenol structurally identical to eugenol, but with a propyl tail rather than a propylene tail. As such, 4-propylguaiacol can be used interchangeably for many of the reactions being examined. Integration of the 1505 cm^{-1} ring-breathing stretching vibration of the guaiacol core revealed that consumption of the methoxyphenol substrate was highly dependent on the use of water or its deuterated derivative (Figure 19).

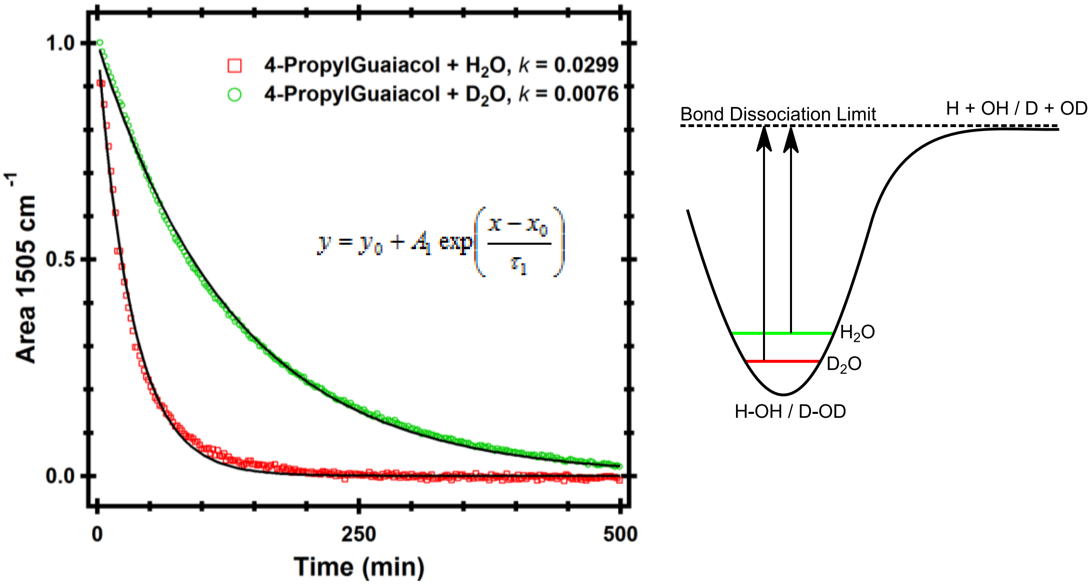

Figure 19. Kinetics curves of the closs of the 1505 cm^{-1} ring breathing stretching vibration over the course of photolysis of 4-propylguaiacol and eugenol on rutile in water and D_2O humidified atmospheres are shown. The deuterated water affected a much slower rate than the regular water suggesting a primary kinetic isotope effect. The kinetic curve of the eugenol under water is shown for comparison. This is known as the kinetic isotope effect, due to a difference in zero point vibrational energies of the OH and OD bond as demonstrated in the curve above.

The D_2O humidified studies of 4-propylguaiacol's photolysis showed a significantly lower rate constant than that of the H_2O studies. It was concluded that a kinetic isotope effect was present for the photoreaction of eugenol on rutile involving water. The kinetic isotope effect is a difference in kinetics (rate) of a reaction when a heavier isotope of an element involved in the rate determining step of a reaction is used rather than the more common isotope. In the case of the deuterium vs hydrogen question, the difference in rate of consumption of the

4-propylguaiacol between the H_2O and D_2O despite relatively similar IR profiles at the 100 minute time point indicates that water indeed plays a key role in the rate limiting steps of the reaction insofar as the formation of the hydroxyl radical is a rate limiting step.

3.2 Gas Cell IR sealed chamber experimentation

In order to help elucidate the identities and structures of these observed products on the rutile surface, studies of the gas-phase products of the photoreaction were conducted in an improvised sealed reaction vessel to obtain clean reaction spectra of these gaseous products. IR spectra attained in this experiment showed only two principal IR absorptions at 2360 and 2340 cm^{-1} indicative of carbon dioxide formation as seen in Figures 20 and 21 below.

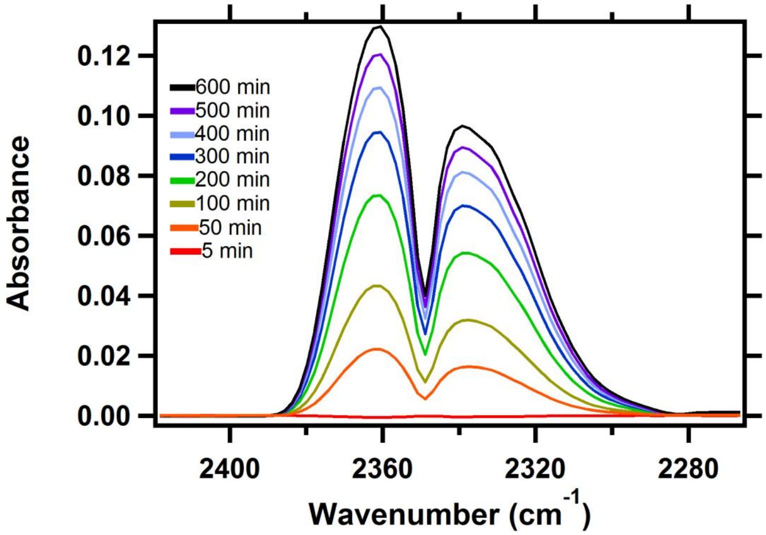

Figure 20. The gas-phase IR spectra of carbon dioxide formed from the photolysis of eugenol on rutile over 600 min are shown. No other infrared bands above the noise were detected in the gas cell.

Kinetics analysis of this region via equation 3 yields a calculated rate constant of 0.00441 min^{-1} (Figure 21).

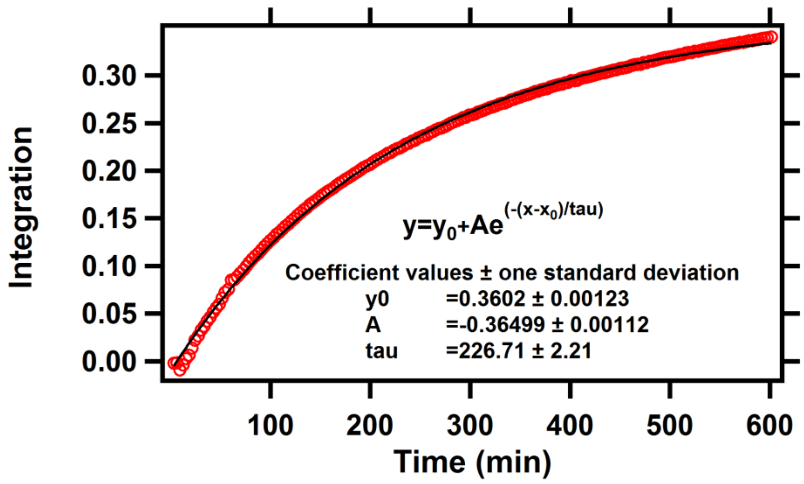

Figure 21. The kinetics analysis of the CO_2 peaks shown in Fig 20

Interestingly, the rate of CO_2 production was less than the rate of loss of eugenol observed by loss of the 1505 cm^{-1} peak seen in Fig 18. This could suggest that not all of the eugenol loss observed is reactive, or, as the other kinetics analyses suggest, some persistent condensed-phase oxidation side products such a oxalate are formed while main products such as the coniferyl aldehyde intermediates are formed.

3.3 Condensed-phase product collection studies

3.3.1 Eugenol on rutile (72 h exposure) produces vanillin, coniferyl aldehydes, and vanillic acid

With gas-phase infrared spectroscopy indicating that the primary gaseous species formed is indeed carbon dioxide, there was great interest in the nature of the products forming on the surface and remaining there during the photolysis period. As such, larger scale condensed phase studies of these photolysis reactions were performed such that extraction and analysis by GC-MS was feasible for preliminary product identification. The total ion chromatogram (TIC) of the extracted and functionalized products of eugenol's photolysis on rutile in a humid (>30%) atmosphere are shown below in Figure 22.

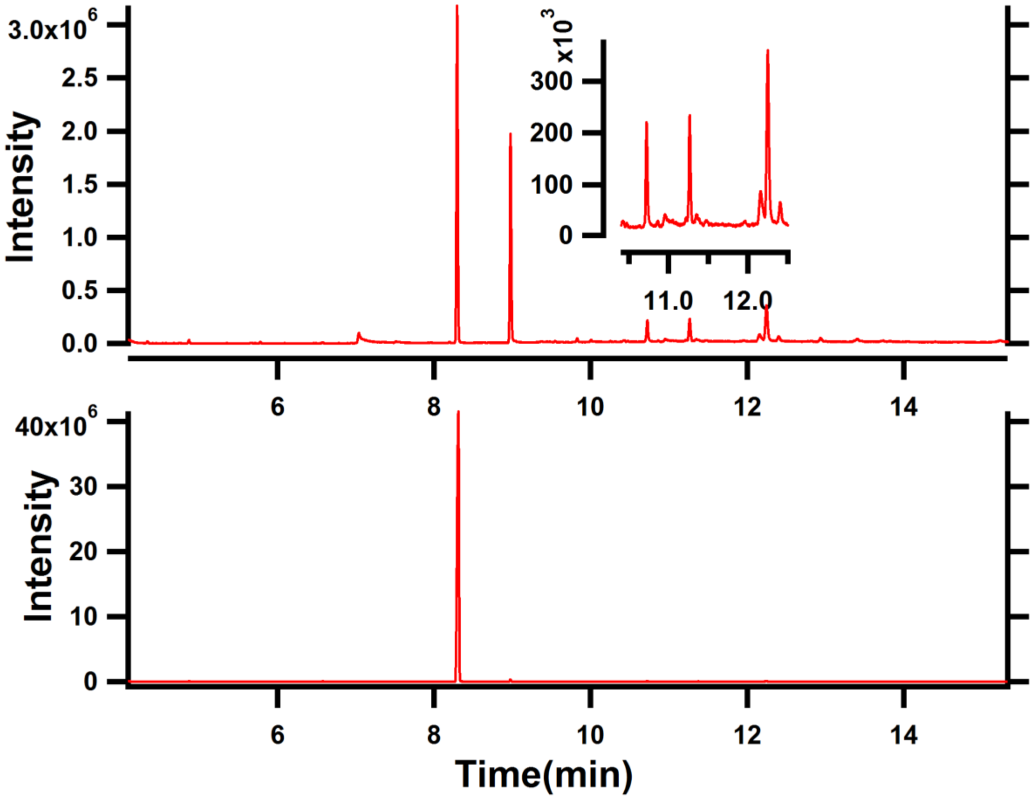

Figure 22. The GC chromatograms of the products of eugenol photolysis on rutile extracted into acetonitrile and functionalized with BSTFA (control-bottom, experimental-top). Compounds as identified by NIST library search algorithm include: Eugenol, 8.291 min; Vanillin, 8.978 min; E/Z-coniferyl aldehyde, 10.720 min, 12.248 min; vanillic acid, 11.261 min; unidentified m/z=280, 12.153 min; unidentified m/z=297, 12.397 min.

Despite initial notions from IR studies that only a limited number of products were forming at the surface, the condensed-phase studies showed a wealth of products resolvable by GCMS via matching to the NIST Mass Spectrometry Library, despite a large amount of unreacted eugenol remaining. The mass spectra of the four most abundant product peaks can be seen collected in Figure 23.

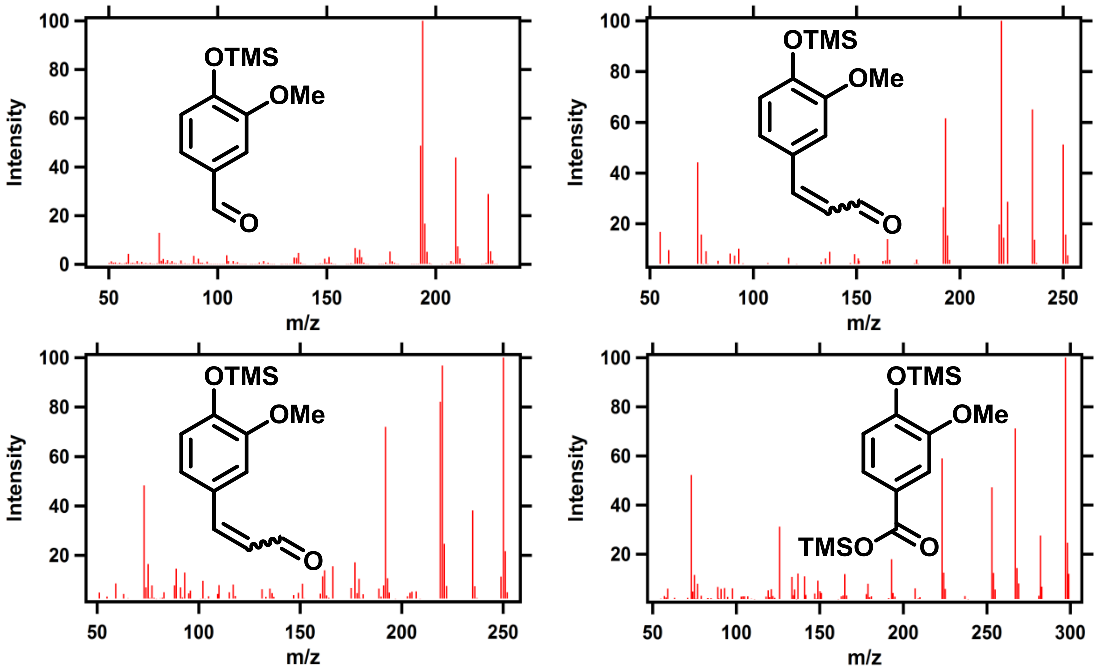

Figure 23. Shown above are the mass spectra of the four major product peaks observed following the photolysis of eugenol. Products are functionalized (TMS group added by BSTFA) to increase volatility. Clockwise from the top left: vanillin, E/Z coniferyl aldehyde, vanillic acid, E/Z coniferyl aldehyde. The two coniferyl aldehydes are surmised to be stereoisomers due to their incredibly similar MS fingerprints, but the algorithm cannot differentiate which is which (E vs Z).

These four products all suggest oxidation and/or loss of the propenyl tail on the original eugenol structure, allowing some insight into the mechanism by which this reaction may occur. The hypothetical mechanism shown in Figure 24 was generated using intuitive thoughts by Augugliaro et al[23].'s work as a template upon which to build. Additional work by Augugliaro[15] et al. detailed addition of O_2 and reactions of the peroxyl radical, including peroxycyclization and collapse contributed to the hypothesis of the final steps to vanillin synthesis.

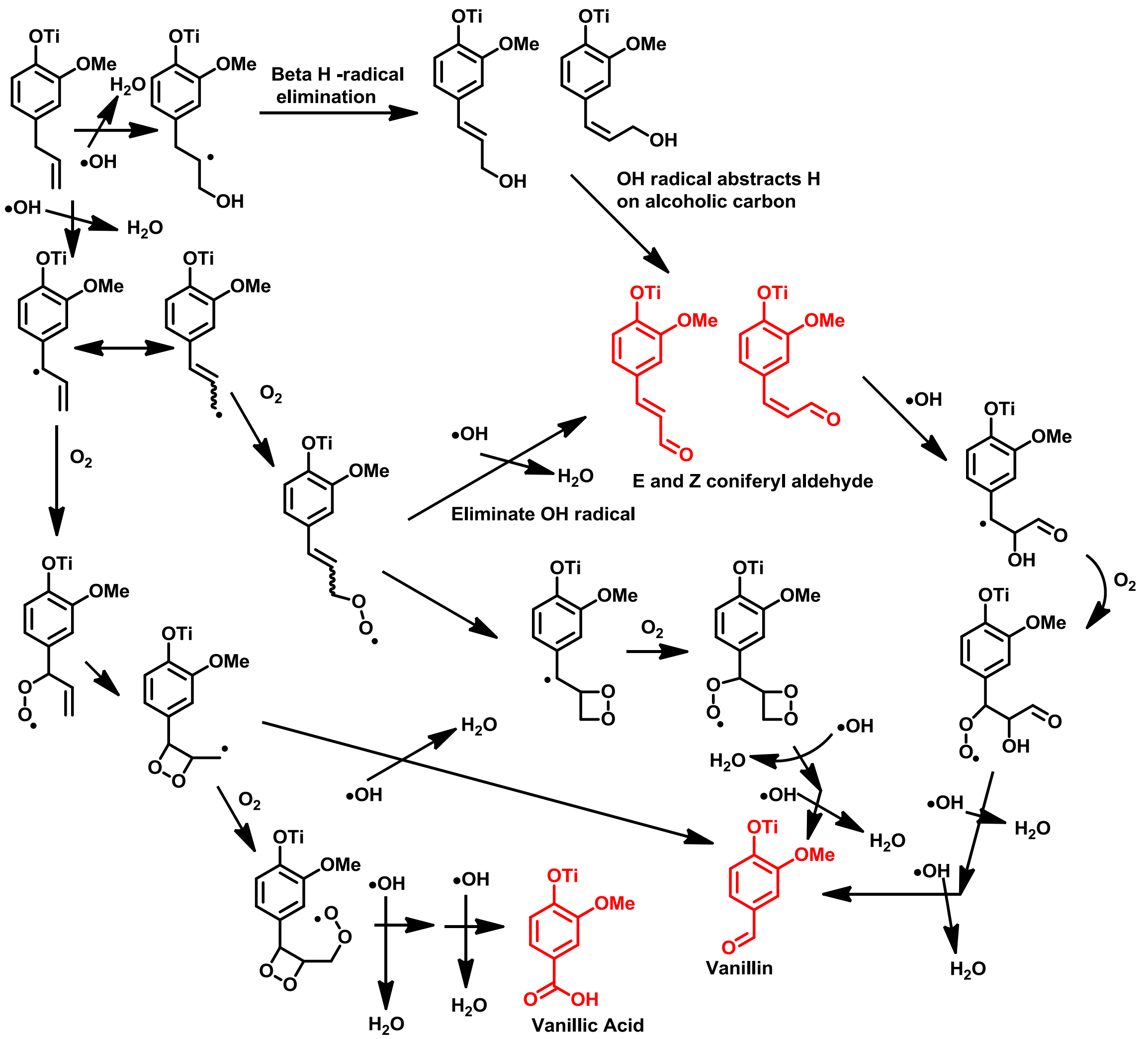

Figure 24. A hypothetical mechanism for the synthesis of the products detected by GC-MS is shown. The initial step would in these scenarios be attack on the alkene or abstraction of the benzylic hydrogen by a hydroxyl radical, followed by alkene rearrangement or radical elimination, then addition of molecular oxygen, allowing oxidation via dioxetane species. The species are all shown with "OTi" rather than "OH" to indicate that they are surface bound. Decomposition pathways of the peroxy radical and subsequent dioxetane are hypothesized using work of Pryor and Porter[26]

It is critical to note that the mechanisms depicted in Figure 25 are highly speculative proposals for the formation of the observed products, and to corroborate these predictions, other systems must be investigated. This mechanism is consistent with the observations made in the condensed phase IR studies. First, the hydroxyl radical is formed from liberation of a bound surface hydroxyl on the rutile via the photocatalysis mechanism shown earlier. This is the rate limiting step of the reaction and is key to all steps that follow. The nascent OH radical than can do one of two modes of attack on the bound eugenol: abstraction of the benzylic hydrogen to form water and a benzyl radical or cleavage of the alkene pi bond to form an alpha hydroxyl alcohol. These newly formed alkyl radicals quickly snatch up a dioxygen molecule from the atmosphere forming a peroxyl radical. This is the source of the oxygen dependence of the reaction observed in the IR studies. Once the peroxyl radical is formed, there's no stopping this reaction. Through some clever electron dancing, eventually a 1,2 dioxetane ring is formed, which spontaneously collapses to produce the aldehyde carbonyl and simultaneously cleave a carbon-carbon bond. Vanillin, the primary condensed-phase end product of this reaction, can be formed from both of the product streams. The other products observed by GC-MS, the two stereoisomers of coniferyl aldehyde and the vanillic acid, are produced by divergence from the vanillin production sequence by means of radical resonance or secondary O_2 adduction. The merits of this reaction scheme were tested by GC-MS analysis of the 4-propylguaiacol system lacking the alkene. The products predicted by these mechanisms help to explain the growth and disappearance of the carbonyl peak over the course of the experiment. What may be occurring is that the coniferyl aldehydes may be forming initially in large quantity and then are steadily converted to the vanillin final product by further radical oxidation. The vanillin carbonyl peak may be masked by trapping of vanillyl alcohol (or a radical analogue thereof) at the rutile surface as shown crudely in Figure 25.

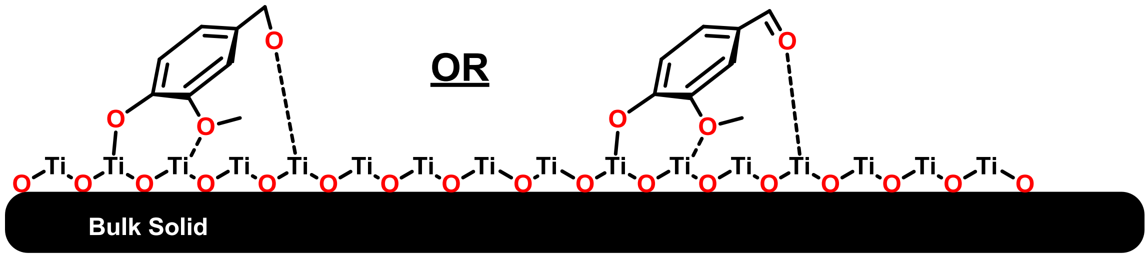

Figure 25. A proposed reasoning for the loss the carbonyl peak upon further oxidation of nascent coniferyl aldehydes is shown above. The "vanillyl alcohol"-like radical species generated from immediate collapse of the dioxetane ring may be transiently stabilized by association with Lewis acidic titanium sites on the rutile surface. Alternatively, the vanillin may form fully and the aldehyde oxygen then associates with the Lewis acidic Ti site, altering carbonyl frequency significantly and non-uniformly depending on number of associated Ti centers.

3.3.2 4-propylguaiacol on Rutile (72 h exposure) produces guaicylethanone and isoeugenol as a reactive intermediate

Repeating trials with 4-propylguaiacol in place of eugenol afforded a different set of products entirely as seen in the GC chromatogram in Figure 26.

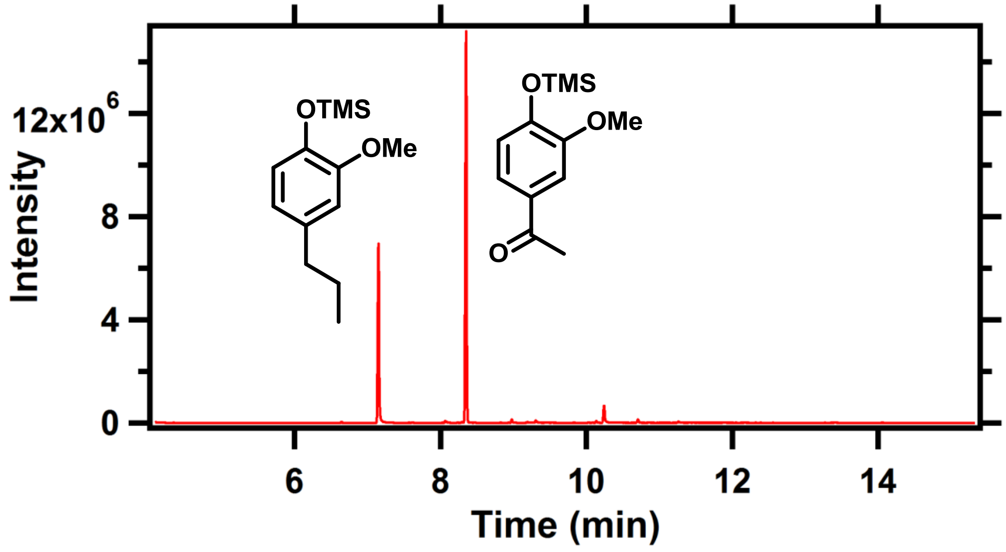

Figure 26. The GC Chromatogram of the products of 4-propylguaiacol photolysis on rutile are shown. Notable peaks include: 4-propylguaiacol, 7.148 min; isoeugenol(trace) 8.035 min; 2-hydroxy-1-guaiacylpropan-1-one, 8.345 min; vanillin(trace) 8.974 min, (guaiacyl core present, m/z =254.1) 10.24 min.

The 4-propylguaiacol products were markedly different than those seen with the eugenol photoreaction, suggesting something very interesting about the mechanism responsible. Suspicious that some of the products may not have desorbed from the rutile, the powder was extracted a second time using BSTFA (bis-trimethylsilyltrifluoroacetamide) to encourage displacement of the alkoxy residues from the surface. During reaction, methoxyphenols are primarily bound to the rutile surface as shown in Figure 27.

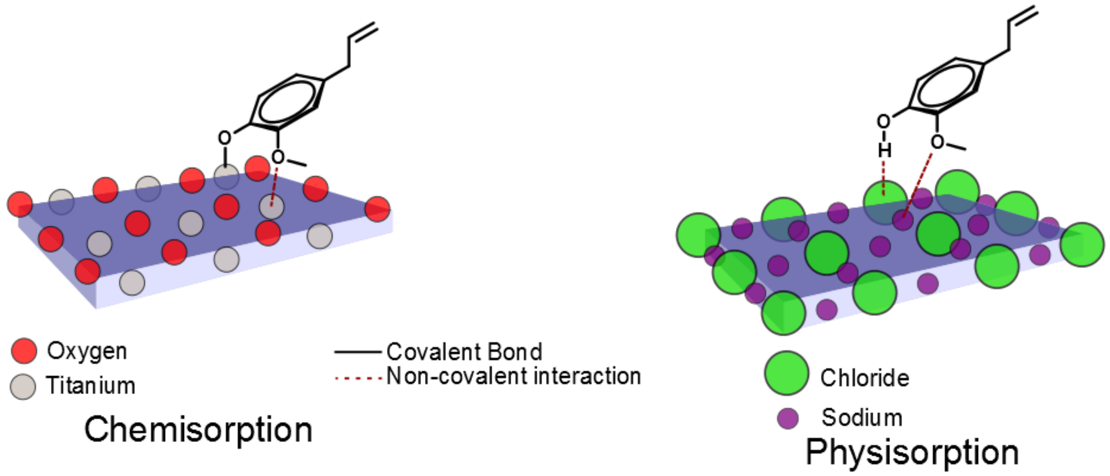

Figure 27. The typical binding mode of methoxyphenols on rutile (chemisorptions) and sea salts (physisorption) are shown above.

This resulted in an incredibly interesting find: isoeugenol was found in very large relative concentration amongst the products isolated from the second extraction (Figure 28). Unusually, some of the products observed seemed to be TMS-derivitized while others did not. The explanation for this disparity may simply be that not enough BSTFA was added to the extract to completely functionalize all free OH groups present, as many OH surface hydroxyls likely exist on the rutile solvent or rutile gas interface as shown in Fig 27.

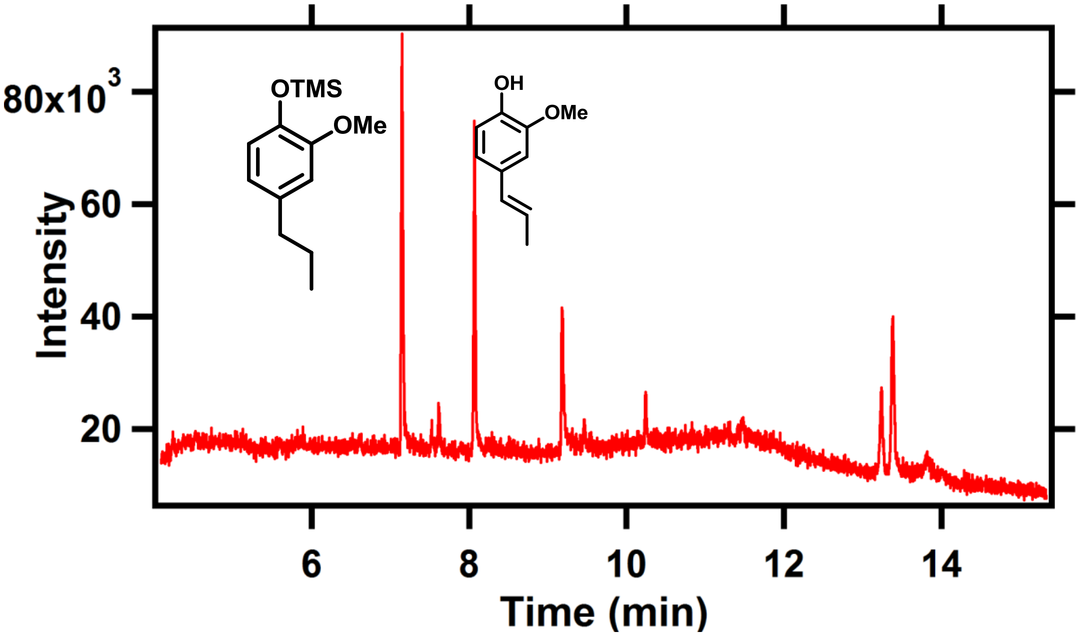

Figure 28. The GC chromatogram of the secondary extraction of the 4-propylguaiacol photolysis products is shown. Notably, 4-propylguaiacol is the predominant peak, but isoeugenol (8.035 min) occurs in large amounts as well. The unknown m/z 254.1 peak at 10.24 min was present as well. Additionally, three other large peaks (all containing the guaiacyl core MS pattern) were present at 9.183 (same pattern as 10.24 min, theorized to be 10.24 sans TMS) min, 13.234 min (m/z =207.1), and 13.375 min (m/z =211.2).

As seen in Figure 27, the secondary extraction afforded a wealth of additional products which help elucidate the mechanism of reaction through their structures. Particularly notable is the large amount of isoeugenol present in the sample. Referring back to Fig 24, isoeugenol derivatives are key intermediates in a number of the hypothesized pathways and potentially provide leads to the mechanism of oxidation in the 4-propylguaiacol reaction. Mass spectra of some of the most abundant tentatively identified products are shown in Figure 29 below.

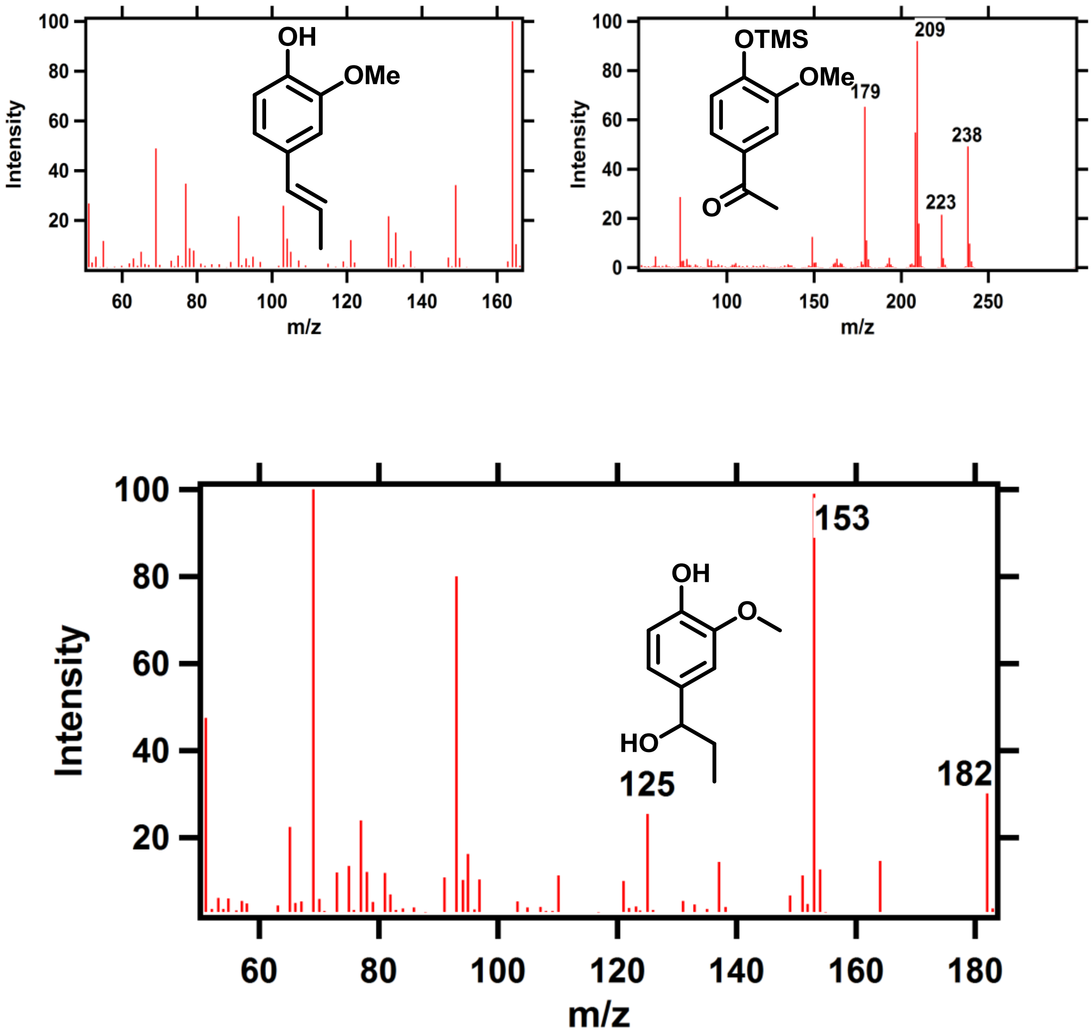

Figure 29. The mass spectra of isoeugenol (upper left), 1-guaiacylethanone (upper right, 65% NIST match, loss of acetyl methyl seen, m/z = 223, parent ion mass match, loss of ether methyl +acetyl methyl m/z=209), and an unknown product m/z = 182 (bottom). Intensities are scaled to the base peak for all three. Results were muddied by incomplete derivitization occurring with the isoeugenol (85% match to NIST library) showing little protection, while the 1-guaiacylethanone appeared almost exclusively as the protected alcohol. It is theorized this differential protection is due to reactivity preference of the alcohol. Because this reaction was extracted for a longer time period than others, non-derivatized substrates could leach into the supernatant. The closest spectral match to the uncertain peak was guaiacylpropanol (Shown in inset). This ID shows some merit (loss of 29 m/z fragment would be alpha C_2H_5 loss, loss of 59 m/z (C_3H_7O) is close to the observed loss of 57 observed, but the fingerprint to library match was below 40% calling into question the identity.

Using this new information a tentative mechanism for the formation of the guaiacylethanone was proposed with isoeugenol as a secondary product as shown in Figure 30 below.

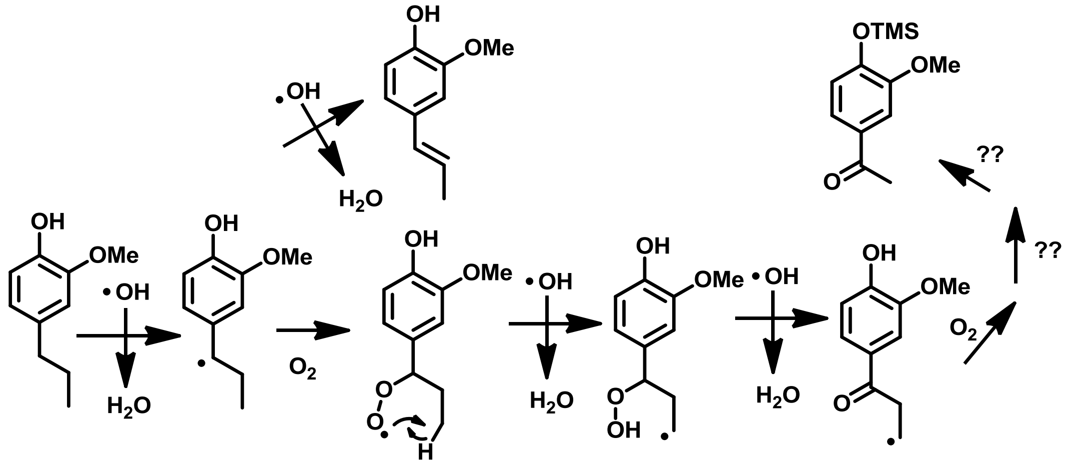

Figure 30. A proposed mechanism for the photooxidative formation of 1-guaiacylethanone and isoeugenol from 4-propylguaiacol is shown above. A hydroxyl radical initiates the mechanism by abstraction of a benzylic proton, which allows radical elimination to form the isoegeunol. Hydroxyl radical attack on the nascent double bond allows adduction of O_2 forming a peroxy radical which collapses to a ketone, eliminating a hydroxyl in the process.

Using the principles of radical molecular oxygen oxidation laid forth by Auguliaro[19] and Pryor and Porter[26], the 4-propylguaiacol can be oxidized to the guaiacylpropanone, but at that point the mechanism by which one carbon is eliminated to form the guaiacylethanone is unclear. Tentative identification (<40% match to NIST MS library fingerprint) of one of the unknown peaks (m/z =182, 9.183 min in Fig 28), seems to indicate that the guaiacyl propanol may form. Perhaps bidentate adsorption of this guaiacyl propanol allows trapping of an enolate analog exposing the methyl cap of the propyl tail to oxidation to CO_2. To make any claims beyond pure unadulterated speculation would be disingenuous.

3.3.3 4-propylguaiacol reacted for a longer time period produces chiefly 1-guaiacylethan-1-one

As an experimental test of the long term end products of this reaction, the 4-propylguaiacol photooxidation was repeated with a 128h exposure compared to the standard 72 h exposure (Figure 31).

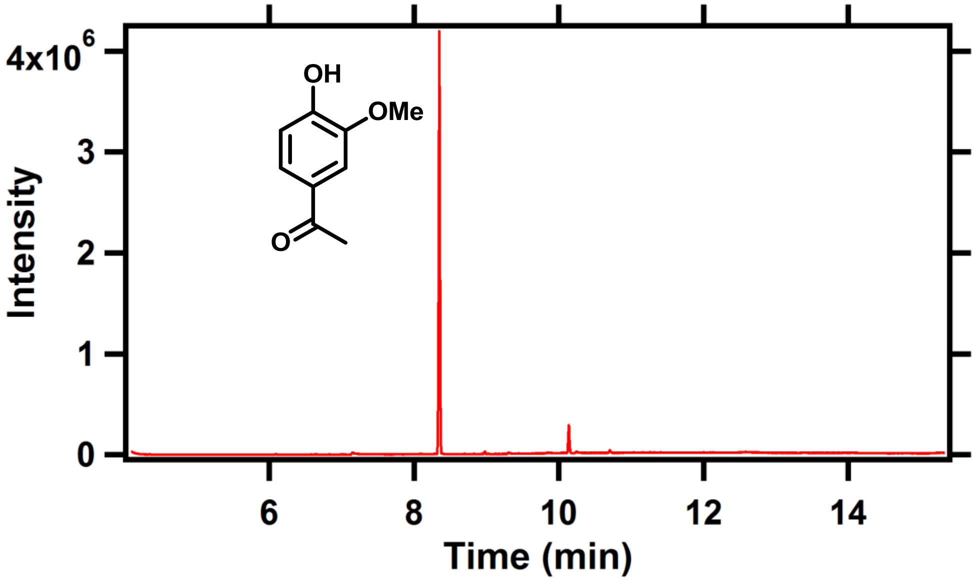

Figure 31. The GC chromatogram of the extracted products of 4-propylguaiacol on rutile following 128h of exposure is shown above. Only two peaks are observed with no residual 4-propylguaiacol detected. The notable peaks included: 8.347 min (MS fingerprint matched 1-guaiacylethan-1-one) and 10.24 min (m/z =254.1 guaiacyl core present).

These results suggest that the isoeugenol pathway for this substrate tends to form only two products in appreciably quantities following long term irradiation. This provides basis for further research into the endgame photolysis products of related methoxyphenolic compounds on the rutile system.

3.3.4 4-methylguaiacol's photoreaction yields chiefly vanillin and vanillol

Finally, as a proof of concept using the simplest alkyl guaiacol, 4-methylguaiacol was reacted under the same conditions as the 4-propylguaiacol and eugenol experiments. Products of the reaction were determined to be vanillin and vanillol (Figure 32).

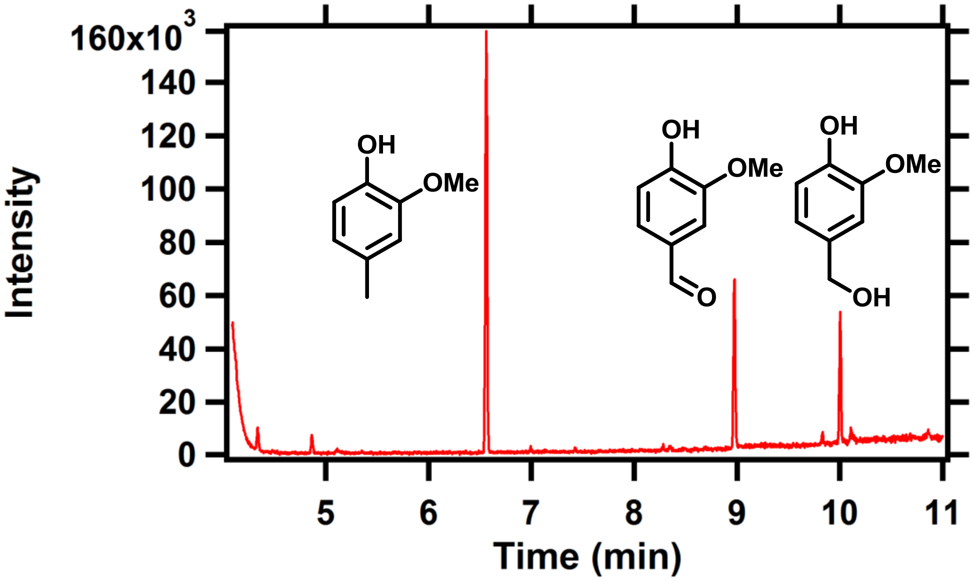

Figure 32. The GC chromatogram of the products of 4-methylguaiacol's photolysis is shown above. Notable peaks include: 4-methylguaiacol, 6.562 min; vanillin, 8.978 min; vanillol, 9.996 min.

The tentative mechanism for this transformation, hypothesized using logic similar to that used to generate mechanisms for the eugenol photooxidation, is shown below in Figure 33.

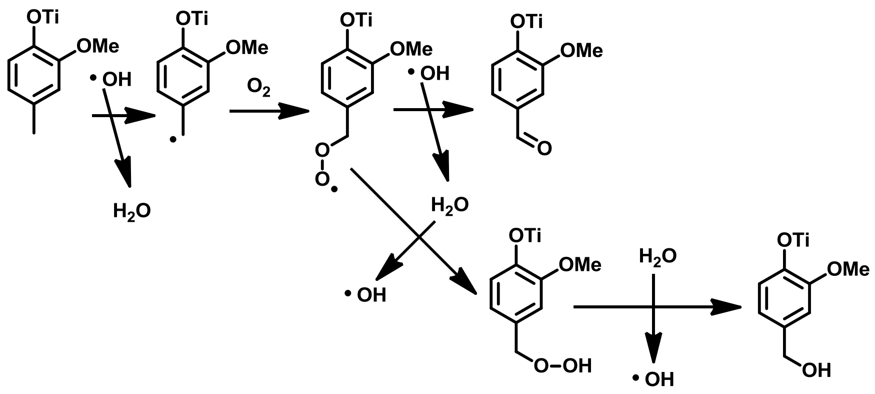

Figure 33. A proposed mechanism for the radical photooxidation of 4-methylguaiacol is shown above. Following hydrogen abstraction and O_2 adduction, the product stream produces primarily vanillin and vanillol.

4. Conclusions

Bringing together the observations from all three model methoxyphenols, one can draw a number of tentative conclusions.

- If the alkyl chain is longer than one carbon and lacks a double bond, the benzylic hydrogen will likely be abstracted by radical attack allowing formation of isoeugenol as a reactive intermediate.
- If the alkyl tail has a double bond, it can be the site of hydroxyl radical attack, allowing formation of a peroxy radical with the addition of oxygen. This peroxy species may then serve as a gateway intermediate for rapidly eliminating carbons of the tail as CO_2 and other low MW gasses via collapse of a dioxetane ring.
- Alternatively, the attack on the double bond also allows formation of an internal double bond via radical elimination, giving an isoeugenol-like intermediate.

These findings present an exciting set of new developments in the context of broader atmospheric chemistry. Photochemical production of vanillin, coniferyl aldehydes and other oxidized methoxyphenolic compounds provides an entry point for many well-documented browning, or albedo reducing, reactions, such as condensation with amines, to occur. This alone emphasizes the importance of study of heterogeneous photocatalysis in the context of aerosol substrates. Additionally, data from this thesis contributes to knowledge of atmospheric lifetimes species structurally similar to the lignin pyrolysis products ecamined. As reaction with OH radical is the primary metric used for lifetime calculations, knowledge of reactivity post hydroxyl radical reaction is also key. Outside of the atmospheric picture, this research opens the door to a number of fascinating possibilities in the field of green chemistry. The transformations afforded by this photoreaction are often done industrially on enormous scale, in solvent, with harsh or costly oxidizing agents specific to the substrate of interest. By tuning the reactivity of this system with doping of other minerals and/or elements, the photoreaction produces a far less environmentally deleterious option for the production of high demand commodity chemicals such as vanillin. What truly would set this apart though is that although production of vanillin can be done in aqueous suspension as shown in Augugliaro's[15] work, a solventless photoxidation reaction would prove even more green. At first glance rutile may seem like just another boring mineral, but its photochemistry proves that it is anything but.

---

[1] Hidy, G.M. *Aerosols, An Industrial and Environmental Science*. Academic Press, 1984.

[2] Penner, JE et al. Aerosols,their direct and indirect effects. In *Climate Change 2001: The Scientific Basis*.; IPCC; University Press: New York, 2001; 291-336

[3] Calvo,A.I. et al. *Atmos. Res.* **2013**, *120-1*,1-28.

[4] Mogili, P.K.; Yang, KH; Young, MA; Kleiber, PD, Grassian, VH. *Atmospheric Environment*. **2008**, *42,* 1752-1761.

[5] Park, R.J. et al. *J. Atmospheric Environment.* **2010**, *44,* 1414-1421.

[6] Woodill, L.A..; Hinrichs, R.Z., *Phys. Chem. Chem. Phys.*, **2010**, *12*, 10766-10774.

[7] Barnum, T.; Medeiros; N. Hinrichs, R.Z. *J. Atmospheric Environment.* **2012**, *55*, 98-106.

[8] Updyke, K.M.; Nguyen, T.B.; Nizkordov, S.A. *J. Atmospheric Environment.***2012**, *63*, 22-31

[9] Shen D.K. et al. *Bioresource Technol.* **2010**, *101,* 6136-6146

[10] O'Neill, E; Kawam, AZ.; Hinrichs, RZ. 244th ACS National Meeting Abstracts, Philadelphia, PA, August 19th-23rd, 2012. COLL230.

[11] Cedillo-González, E.I. et al. *Build. Environ.* **2014**, *71*, 7-14.

[12] Nakata, K.; Fujishima, A. *J. Photoch. Photobio. C.* **2012**, *13,* 169-189.

[13] Bannerji, M.; Tyagi, R. *Current Science* **2006**, *90* (10), 1121-1139.

[14] Hirakawa, T.; Yawata, K.; Nosaka, Y. *Appl. Catal. A.* **2007**, *325,* 105-111.

[15] Augugliaro, V; et al. *Journal of Photochemistry and Photobiology C: Photochemistry Reviews* **2012.** *13:* 224– 245.

[16] M.C. Blount, J.A. Buchholz, J.L. Falconer, *J. Catal*. **2001.** *197*, 303–314.

[17] X. Ye, D. Chen, J. Gossage, K. Li, J. *Photochem. Photobiol. A: Chem.* **2006**. *183*, 35-40.

[18] Bui, T.D.; Kimura, A; Higashida, S; Ikeda, S.; Matsumura, M. *J. Am. Chem. Soc.* **2010.** *132,* 8453–8458.

[19] Augugliaro, V; Camera-Roda, G; Loddo, V; Palmisano, G; Palmisano. *Chemical Engineering Journal*. **2013**. *224*: pp. 136-143.

[20] 2-methoxy-4-propylphenol / 4-propylguaiacol, used as a control for eugenol's exocyclic allyl moiety in the reaction.

[21] DRIFTS = Diffuse Reflectance Infrared Fourier Transform Spectroscopy

[22] Peiró, A.M.; ,Ayllón, A; Peral, J; Doménech, X. TiO_2 photocatalyzed degradation of phenol and ortho-substituted phenolic compounds. *Applied Catalysis B: Environmental.* **2001**, *30:* 359-373.

[23] Augugliaro, V; Camera-Roda, G; Loddo, V; Palmisano, G; Palmisano, L; Parrino, F; Puma, MA. *Applied Catalysis B: Environmental*. **2012**, *111-2*, 555-561.

[24] Bui, T.D.; Kimura, A; Higashida, S; Ikeda, S.; Matsumura, M. *Catalysis B: Environmental*. **2011**. *107*: 119-127.

[25] Diffuse Reflectance Infrared Fourier Transform Spectroscopy

[26] Pryor, W. A. and Porter, N. A. *Free Rad. Biol. Med*. **1992,** *8*, 541-543.